CHAPTER 15: USE OF DISCRETE-DYNODE SECONDARY ELECTRON MULTIPLIERS WITH FARADAYS – A '*REDUCED VOLUME*' APPROACH FOR *IN SITU* U–Pb DATING OF ACCESSORY MINERALS WITHIN PETROGRAPHIC THIN SECTION BY LA–MC–ICP–MS

Antonio Simonetti, Larry M. Heaman & Thomas Chacko
Department of Earth and Atmospheric Sciences, University of Alberta,
1–26 Earth Sciences Building,
Edmonton, Alberta T6G 2E3 Canada
antonio.simonetti@ualberta.ca

INTRODUCTION

Recent U–Pb isotope studies of accessory minerals (*e.g.*, zircon, monazite, titanite) using laser ablation multicollector inductively coupled plasma mass spectrometry (LA–MC–ICP–MS) have made significant advances in generating precise and accurate age data (*e.g.*, Horstwood *et al*. 2003, Simonetti *et al*. 2005, 2006). In particular, the advent of MC–ICP–MS instruments housing multiple ion counting devices (electron multipliers) have provided improvement with regards to the quality of the Pb–Pb or Pb–U isotope data relative to spatial resolution (*i.e.*, lower total volume of sample material consumed). For example, Willigers *et al*. (2002) and Paul *et al*. (2005) conducted *in situ* common Pb isotope measurements by LA–MC–ICP–MS involving a combination of multiple Faraday detectors and one or two electron multipliers, respectively; the latter measured either the ^{204}Pb or ^{202}Hg ion beams. In contrast, Souders & Sylvester (2008a, 2008b) reported on LA–MC–ICP–MS investigations of the common Pb isotope ratios for silicate glasses using a multiple electron multiplier detection system involving five channeltrons housed within a Finnigan Neptune MC–ICP–MS instrument.

The studies of Simonetti *et al*. (2005, 2006) employed MC–ICP–MS instrumentation (NuPlasma from Nu Instruments, Wrexham, UK) housing an innovative collector block containing a combination of twelve Faraday collectors and three discrete-dynode electron multipliers. The three electron multipliers housed within the 'U–Pb collector block' of the NuPlasma instrument at the University of Alberta permit acquisition of low $^{207, 206, 204}$Pb ion signals (between ~1 and ~30 millivolts – Faraday bucket ion signal equivalent) with high precision and consequently laser ablation analyses consume relatively small sample volumes. Figure 15-1 compares the precision *versus* sample consumption of the protocol described here to those of other analytical methods including other LA–(+/–MC)–ICP–MS configurations, sensitive high resolution ion microprobe (SHRIMP), and isotope dilution thermal ionization mass spectrometry (ID–TIMS). A typical 30-second laser ablation analysis of zircon at a fluence of ~2 J/cm^2 (~0.03 mJ pulse energy), 20–40 μm diameter, and 4 Hz repetition rate produces a pit depth between ~5 and ~10 μm (Fig. 15-2); this is markedly less than the thickness of a standard petrographic thin section (~30 μm). The U–Pb date of 1835.7 ± 4.7 Ma (2σ; Fig. 15-2d) obtained by the repeated laser ablation analysis (n = 10) of a single zircon from a petrographic thin section of sample LH94-15 (Fig. 15-2; Simonetti *et al*. 2006) is indistinguishable from its ID–TIMS age

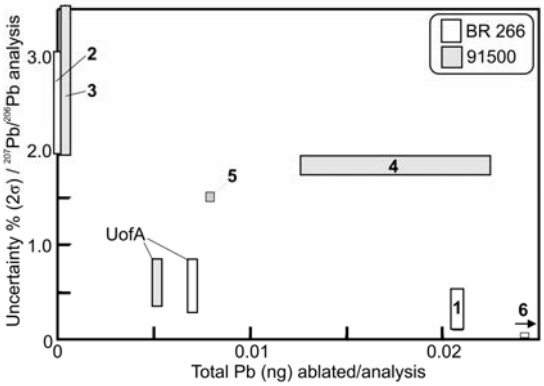

FIG. 15-1. Comparative plot illustrating the typical uncertainty (internal precision, 2σ) associated with the ^{207}Pb/^{206}Pb measurement *versus* the total amount of Pb (ng) ablated for international zircon standards BR266 and 91500 using various laser ablation–ICP–MS instrument configurations and SHRIMP analysis. 1, MC–ICP–MS (all Faraday bucket configuration: Simonetti *et al*. unpublished BR266 data); 2, SHRIMP (Stern 2001); 3, LA–quadrupole (Cox *et al*. 2003); 4, LA–quadrupole (Jackson *et al*. 2004); 5, LA–quadrupole (Jeffries *et al*. 2003); 6, range of ~3 to 11 ng of total Pb by ID–TIMS (Stern 2001); UofA = Pb consumed using the protocol described here. Diagram taken from Simonetti *et al*. (2005).

Mineralogical Association of Canada Short Course 40, Vancouver, B.C., p. xxx–xxx

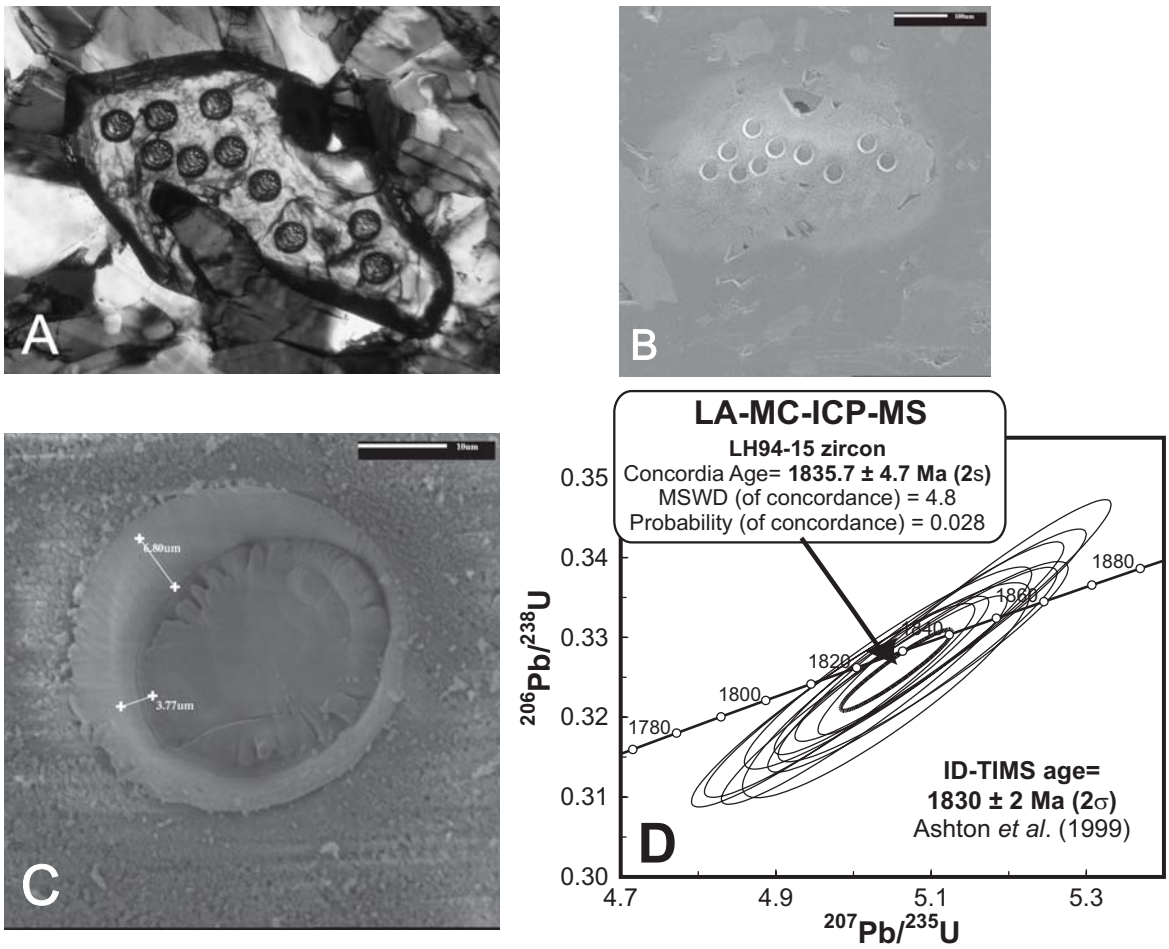

FIG. 15-2. **A**, Photomicrograph of a petrographic thin section of enderbite sample LH94-15 (source of internal zircon standard LH94-15). The photo displays the locations of the 40 μm analysis spots within a large zircon crystal, which is surrounded predominantly by pyroxene, plagioclase, biotite and quartz; **B**, Topographic scanning electron microprobe (SEM) photo of same LH94-15 zircon grain shown in A; **C**, enlarged view of one of the 40 μm laser pits indicating a depth of between ~4 to ~7 microns; **D**, Concordia plot indicating an age of 1835.7 ± 4.7 Ma (2σ) obtained with the 10 laser ablation analyses shown in A. This date is indistinguishable from the ID–TIMS age of 1830 ± 2 Ma (2σ; Ashton *et al*. 1999).

of 1830 ± 2 Ma (2σ; Ashton *et al*. 1999).

The advantages of dating accessory minerals *in situ* within petrographic thin section by LA–MC–ICP–MS cannot be overstated. This approach greatly reduces both sample preparation and analysis time relative to that needed for other geochronological methods. For example, in a typical 8-hour analytical session, 3 to 5 thin sections with 10–20 spots per section can be analyzed using the protocol outlined in Simonetti *et al*. (2006). This '*reduced volume*' *in situ* dating technique also provides the opportunity to link age information directly for a particular sample with deformational fabrics or fine scale textures (*e.g.,* Banerjee *et al*. 2007), and pressure–temperature data derived from electron microprobe analysis of minerals in the same thin section (*e.g.,* Laberge & Pattison 2007). Thirdly, the LA–MC–ICP–MS methodology generates data at significantly lower cost (by a factor of 2 to 4) than is possible with ID–TIMS or SHRIMP.

In this chapter, we describe in detail the instrumentation and important calibration procedures involved in obtaining high quality and accurate geochronological information using the LA–MC–ICP–MS analytical protocol outlined in Simonetti *et al*. (2006). We demonstrate the accuracy of the analytical protocol with several examples of LA–MC–ICP–MS age data obtained on petrographic thin sections for samples also dated by ID–TIMS. As a follow up to our earlier study (Simonetti *et al*. 2006) involving the use of the

standard 30 cm^3 ablation cell, here we conduct analogous U–Pb dating experiments with thin sections using the 33 cm^3 SuperCell™ (also manufactured by New Wave Research). Both ablation cells have similar volumes; however, the geometry and flow characteristics of the SuperCell™ have been specifically designed to enable rapid evacuation of ablated particles in a large cell format (Fig. 15-3). Another important reason for using the SuperCell™ is its capacity to house thin sections and mounts containing matrix-matched external standards simultaneously (Fig. 15-3). This feature permits the use of the 'standard sample' bracketing technique for monitoring the Pb *versus* U laser-induced elemental fractionation (LIEF) without the need to open the ablation cell (hence results in fewer perturbations to plasma conditions during an analytical session and increased productivity).

MC–ICP–MS and laser ablation instrumentation

A summary of instrument parameters used for both the laser ablation system and MC–ICP–MS instrument is listed in Table 15-1. This collector configuration allows for simultaneous acquisition of ion signals ranging from mass ^{203}Tl to ^{238}U, with the ^{207}Pb, ^{206}Pb, and ^{204}Pb ($+^{204}Hg$) ion beams measured on the three electron multipliers (Table 15-2; Simonetti *et al*. 2005). The NuPlasma MC–ICP–MS is coupled to a frequency quintupled (λ = 213 nm) Nd:YAG laser ablation system (New Wave Research, USA) and comparative tests were conducted using both 'standard' and 'SuperCell™' ablation cassettes.

Discrete-dynode electron multipliers. The information relative to the ETP electron multipliers presented in this section is summarized from resource material available at the SGE Analytical

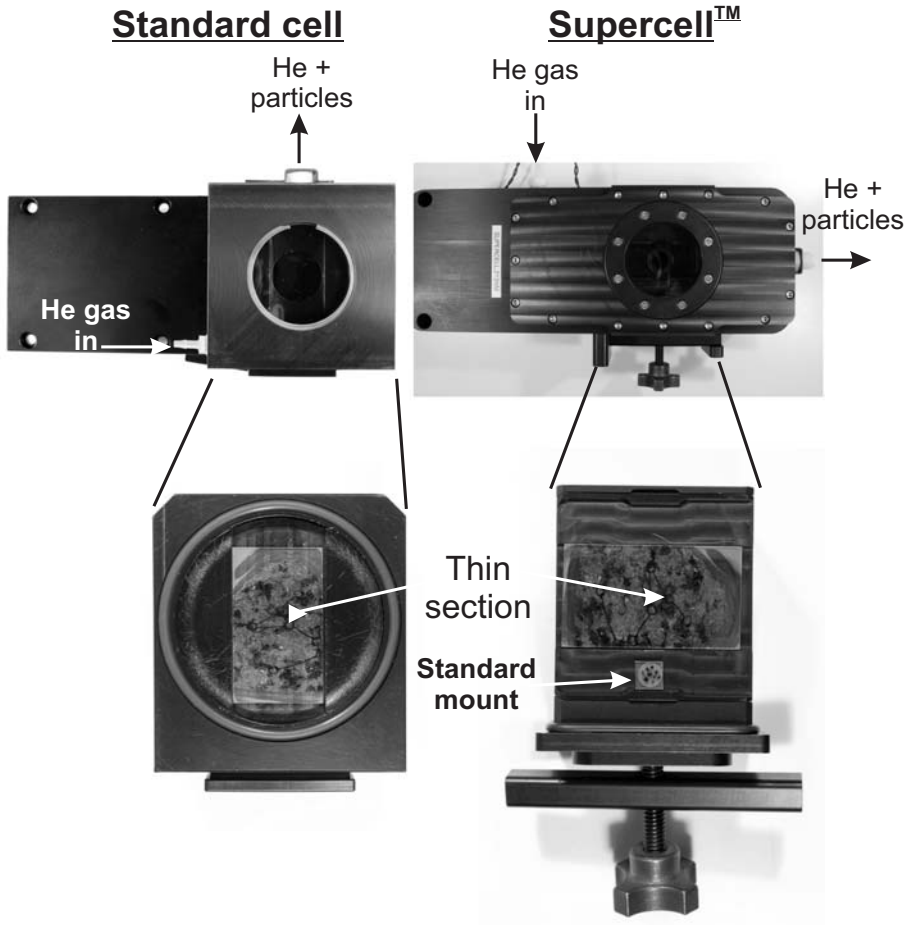

FIG. 15-3. Comparative photographs of the standard ablation cell and Supercell and their corresponding sample holder cassettes from New Wave Research. The larger volume, geometric design of the Supercell allows for the simultaneous insertion of mounts containing standard grains adjacent to the thin section.

TABLE 15-1. OPERATING CONDITIONS AND INSTRUMENT SETTINGS

ICP		**Laser**	
MC-ICP-MS			
Model	Nu plasma from Nu instruments	Model	UP213 Nd:YAG – New Wave Research with aperture imaging system
Forward power	1300 W	Wavelength	213 nm
Reflected power	≤10 W	Max. output energy	3 mJ per pulse @ 20 Hz using a 160 µm spot size
Cool gas flow rate	13 $Lmin^{-1}$ (Ar)	Pulse width	3 ns
Auxiliary gas flow rate	1 $Lmin^{-1}$(Ar)	Energy density	2 -3 J/cm^2
Sample transport:		Focus	Fixed at sample surface
Ablation cell	1 $Lmin^{-1}$(He)	Repetition rate	4 Hz
DSN-100	Membrane – 2.70 to 3.50 $Lmin^{-1}$ (Ar) heated to 110ºC	Spot size	Single spot analysis – 12, 40 µm
	Spray chamber – 0.30 $Lmin^{-1}$(Ar) heated to 110ºC	Ablation cell	30 cm^3 standard cell & 33 cm^3 Supercell™
Nebuliser - DSN	Glass Expansion micromist (borosilicate glass) – 100 µ$Lmin^{-1}$ equipped with Teflon PTFE adaptor & PFA Teflon tubing (1.3 mm OD x 0.25 mm ID)		
Sampler cone	Ni with 1.15 mm orifice		
Skimmer cone	Ni with 0.6 mm orifice		

Conditions and instrument settings are identical for experiments using both the standard and Supercell™ laser ablation cells.

Chemistry Ltd. website (http://www.sge.com). The purpose of an electron multiplier is to detect every ion of the selected mass that has passed through the energy (mass) filter of a mass spectrometer. The basic physical process that allows an electron multiplier to operate is referred to as *secondary electron emission*. When an ion or electron strikes a surface it can cause electrons located within the outer layers of atoms to be released. The number of secondary electrons released depends on the type of incident primary particle, its energy, and characteristic of the incident surface. In general, there are two basic types of electron multipliers commonly used in mass spectrometric analysis: these are *discrete-dynode* (Fig. 15-4) and *continuous-dynode* electron multipliers. The three discrete-dynode electron multipliers contained within the 'U–Pb' collector block of the NuPlasma instrument are manufactured by ETP Electron Multipliers (a division of THE SGE Group). Discrete-dynode electron multipliers amplify the secondary electron emission process by using an array of electrodes referred to as dynodes. Ions hitting the first dynode cause secondary electrons to be emitted from the

TABLE 15-2. CONFIGURATION OF THE 'U-PB COLLECTOR BLOCK' USED FOR LASER ABLATION EXPERIMENTS

EX-H	H6	H5	H4	H3	H2	H1	AX	L1	L2	**IC0**	**IC1**	**L3**	**IC2**	**EX-L**
Faraday	Far.	Far.	Far.	Far.	Far.	Far.	Far.	Far.	Far.	**Discrete dynode EM**	**Discrete dynode EM**	**Faraday**	**Discrete dynode EM**	**Faraday**
^{238}U	^{235}U	----	----	----	----	----	----	----	----	^{207}Pb	^{206}Pb	^{205}Tl	^{204}Pb + (^{204}Hg)	^{203}Tl

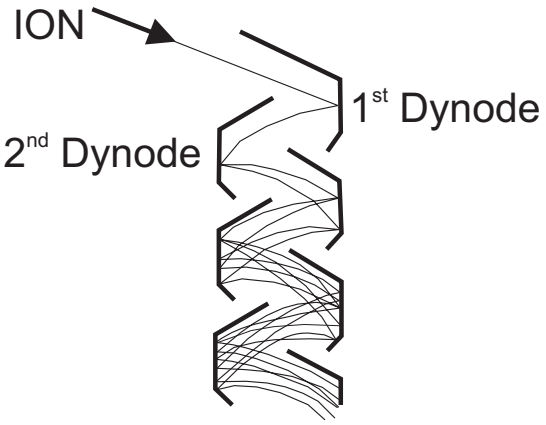

FIG. 15-4. Illustration depicts the ion optics of an ETP discrete-dynode electron multiplier showing the electron gain at each successive dynode. This electron cascading process can result in 'gains' up to 10^8 being achieved with ~21 dynodes (diagram taken from ETP's website at www.etpsci.com).

surface. The optics of the dynodes focuses these secondary electrons onto the next dynode of the array (Fig. 15-4), which in turn emits even more secondary electrons from its surface than the first dynode. Consequently, a cascade of electrons is produced between successive dynodes, with each dynode increasing the number of electrons in the cascade by a factor of 2 to 3; this process is allowed to continue until the cascade of electrons reaches the output electrode where the signal is extracted. A typical discrete-dynode electron multiplier has between 12 and 24 dynodes and is used with an operating 'gain' of between 10^4 and 10^8. For a new (unused) electron multiplier, the gain is achieved with a lower applied voltage (~1800 volts). With time and usage, the surfaces of the dynodes slowly become covered with contaminants from the high vacuum system, which results in a decrease of their secondary electron emission capacity (and consequently drop in 'gain'). Thus, the operating high voltage applied to the electron multipliers must be periodically increased in order to maintain the required multiplier gain. In previous investigations Richter *et al*. (2001) and Hoffmann *et al*. (2005) have conducted detailed investigations of the analytical performances (*e.g.*, linearity, relative yield, stability) of the same ETP electron multipliers employed here primarily for the purpose of U–Th disequilibrium series research using several types of MC–TIMS and MC–ICP–MS instruments. Several of the electron multiplier calibration procedures described here (*e.g.*, determining optimal operating voltage and electron multiplier–Faraday detector calibration) are identical to those reported in both Richter *et al*. (2001) and Hoffmann *et al*. (2005).

The NuPlasma MC–ICP–MS instrument equipped with the U–Pb collector block contains slits that permit passage of ions to the three discrete-dynode electron (ETP) multipliers (labeled IC0, IC1 and IC2), which lie on the low mass side between the last four Faraday collectors (Table 15-2). A small double ESA assembly that deflects the two outer ion beams into off-axes ETP multipliers is located behind the Faraday collector block. In contrast, the central ion beam passes through a slit in the middle part of the Faraday block. There is a small deflection imposed onto the central ion beam to ensure that the multiplier does not lie directly in line with its central channel. The latter offers a simple, but effective means of protecting the ion counters from excessive beams (typically $>10^7$ cps; counts per second) that may be incident on the devices. The multipliers can safely measure signals up to several million counts per second; however, ion signals were kept below 2 x 10^6 cps in almost all of the laser ablation analyses of zircon so as to prolong the longevity of the ETP detectors. The linearity and stability of the ion counters are better than 0.2% during any one analytical session, whereas dark noise is 0.1 cps or less.

Discrete-dynode–Faraday calibration: measurement of $^{206}Pb/^{238}U$ values. As stated earlier, with progressive use, electron multipliers experience degradation in 'gain' and this is compensated by periodic augmentation of the operating voltage. The frequency of the latter procedure is strictly dependent on the use of the electron multipliers; however it is typically in the order of several months. The relative gains ('linearity') between the three electron multipliers (relative to size of the different Pb ion signals) are measured before each analytical session. If these fall below values of 70% and 80% for IC0, IC1 and IC2, respectively, then the operating voltage is increased in order to yield relative gains of ~80% for IC0 and IC1, and ~90% for IC2 (as recommended by Nu Instruments Ltd.). The optimal operating voltage for each electron multiplier is determined by examining the relationship between high voltage and the relative yield (*i.e.*, absolute ion signal), similar to the procedure outlined in Richter *et al*. (2001). A ~1 ppb solution (2% HNO_3) containing the NIST

SRM 981 Pb standard is aspirated continuously and the absolute count rates are recorded at different operating voltage settings for IC0, IC1, and IC2 sequentially. Typical electron multiplier percent yield curves are shown in Fig. 15-5 and these are characterized by 'horizontal operating plateaus' at higher voltage settings for each ion counter. As outlined by Richter *et al*. (2001), the optimal high voltage setting is the area corresponding to the initial segment of the horizontal plateau, or just past the 'knee' of the curve (Fig. 15-5).

The relative gain between IC0 and IC1 (measure ^{207}Pb and ^{206}Pb ion signals, respectively; Table 15-2) has been demonstrated to be extremely linear over a wide range of absolute count rates (Simonetti *et al*. 2005). However, the electron multipliers can become 'non-linear' after prolonged use and at higher operating voltages, the 'linearity' associated with the gain of any individual electron multiplier is lost. Therefore, it is imperative to monitor relative gains of the electron multipliers especially when operating at higher amplifier voltage. The electron multipliers within the NuPlasma instrument at the University of Alberta have experienced extensive use since October 2003 and after four years are now at operating voltages of –2675, –2600, and –2075 for IC0, IC1, and IC2, respectively (starting operating voltages were approximately –2000).

It is also extremely important to monitor the relative gain between electron multiplier IC1 and Faraday collector EX–H, which measure the ^{206}Pb and ^{238}U ion signals, respectively (Table 15-2). Obviously, an accurate assessment of the relative gain between these two detectors is crucial for determining ^{206}Pb/^{238}U values and hence the degree of concordance of mineral standards and unknowns (by comparing the Pb/U and ^{207}Pb/^{206}Pb values). In other words, the relationship (if any) between the absolute ^{206}Pb ion signal recorded on IC1 and calculated ^{206}Pb/^{238}U has to be determined; the calibration procedure described below is conducted subsequent the adjustment and increase of the operating voltages for each electron multiplier as described above.

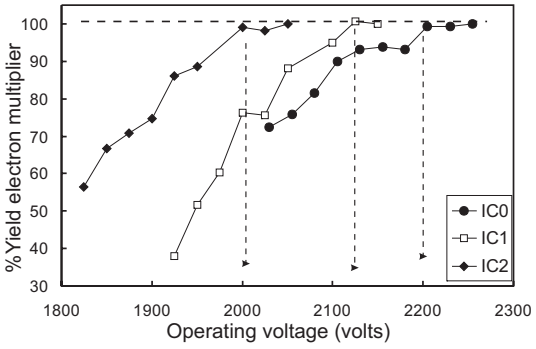

FIG. 15-5. Diagram illustrating the typical %yield for electron multipliers IC0, IC1, and IC2 *versus* the operating voltage setting. The dashed arrows respresent the optimal operating voltage setting located at the initial segment of the 'horizontal operating plateau'.

There are two possible methods for investigating the relationship between the absolute ^{206}Pb ion signal and measured ^{206}Pb/^{238}U values. One approach is to prepare gravimetric solutions with variable concentrations of Pb and U such that the ^{206}Pb ion signal recorded spans the typical range of signal intensities measured in unknown zircons (*i.e.*, between >1 x 10^5 and <2 x 10^6 cps). This approach is similar to that described by Hoffmann *et al*. (2005). An alternative method would involve repeated laser ablation analysis of a well characterized internal zircon standard that yields concordant ages but contains variable Pb and U contents. However, in practice the latter option is currently not feasible because well established, international zircon standards (*e.g.*, BR266, 91500) are characterized by relatively homogeneous Pb and U abundances; thus we have investigated the electron multiplier IC1–EX-H Faraday calibration using the first option.

A 100 ml gravimetric 'shelf' solution (in 2% HNO_3) was established containing Pb (NIST SRM 981) – natural U – Tl (NIST SRM 997) with concentrations of 2 ppb, 25 ppb, and 2 ppb, respectively. The solutions were analyzed using an introduction set up identical to that employed for laser ablation analysis; *i.e.*, laser ablation cell sample-out line (flushed with He gas) is 'Y'–connected to DSN-100 (desolvating nebulizer, Nu Instruments) sample-out line (Simonetti *et al*. 2005). This gravimetric 'shelf' solution was subsequently diluted in different proportions in order to vary the absolute ^{206}Pb ion signal. The measured ^{206}Pb/^{238}U values were then recorded and the results are shown in Figure 15-6. The measured ^{206}Pb/^{238}U values (Fig. 15-6a) and deviation relative to the stoichiometric value of the solution (Fig. 15-6b) are plotted as a function of the absolute ^{206}Pb ion signal. The data in both plots define well constrained arrays (r^2 ~0.97) that can be described by logarithmic equations. Of importance, the deviation is confined to <3% for ^{206}Pb ion signal intensities between ~2.5 x 10^5 and 1.5 x 10^6 cps,

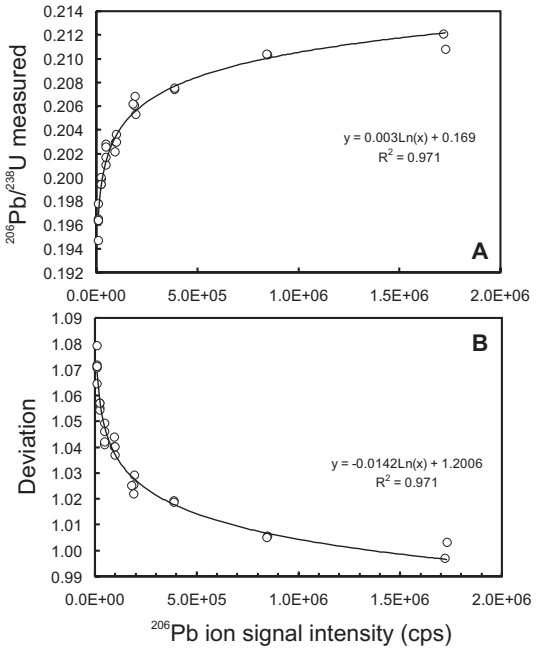

FIG. 15-6. Plots of measured $^{206}Pb/^{238}U$ values (**A**) and deviation factor relative to stoichiometric value (**B**) *versus* ^{206}Pb ion signal intensity in counts per second (cps) obtained for solution mode analyses of a gravimetric shelf solution containing natural U, Pb (NIST SRM 981) and Tl (NIST SRM 997). The same solution was analyzed consecutively with repeated dilutions using 2%HNO_3.

with an increase occurring particularly at extremely low ^{206}Pb ion signal (<5 x 10^4 cps). The equation defined in Fig. 15-6b can then be inserted into an off-line excel data reduction spreadsheet as a correction factor for the $^{206}Pb/^{238}U$ values (and $^{207}Pb/^{235}U$) as a function of the absolute ^{206}Pb ion signal. However, as explained in the Simonetti *et al*. (2005) study, the $^{207}Pb/^{235}U$ values reported are not those measured due to the very small ^{235}U ion signals but instead are calculated by multiplying the $^{207}Pb/^{206}Pb$ and $^{206}Pb/^{238}U$ (both mass bias and blank corrected), and the natural $^{238}U/^{235}U$ value of 137.88 (Steiger & Jäger 1975).

Standard ablation cell versus the 'SuperCell™'–Ion signal decay + 'washout' and 'sensitivity'. Other important features to investigate are the signal 'decay' (relative to Faraday collector EX-H) and particle 'wash-out' times associated with the measurement of the ^{238}U ion signal. This evaluation is critical for certain LA–MC–ICP–MS geochronological applications, such as dating a large population of detrital zircon (*e.g.*, Lemieux *et al*. 2007). For such 'high volume' sample applications, it is important to determine the minimum amount of time required to wait in between individual analyses in order to avoid cross-contamination.

In recent years, use of the standard laser ablation cell with the UP213 system at the University of Alberta was slightly modified in that 1-inch diameter clear plastic inserts were placed within the central hole of the sample mount holder. This is done primarily to eliminate the 'dead' volume located beneath an epoxy mount or thin section being analyzed and hence reduce re-equilibration time (for plasma conditions) subsequent sample exchanges. This practice also increased sensitivity by a factor of at least 2, such that the sensitivity of the standard cell is similar to that obtained with the SuperCell™ design (discussed later; see Fig. 15-8). Thus, the comparative tests described below between the standard and SuperCell™ ablation cassettes were conducted with the 1-inch plastic inserts placed in the former.

Figure 15-7 displays the results of combined 'wash-out' + 'decay' patterns recorded on Faraday collector EX-H (Fig. 15-7a) and electron multiplier IC1 (Fig. 15-7b) subsequent to the standard 30 seconds of laser ablation analysis for various zircon standards (with variable U contents). The in-house zircon standard LH94-15 was ablated using the SuperCell™, whereas the remaining zircon standards were analyzed using the standard laser cell. The analyses of LH94-15 yielded a 4-fold variation in ^{238}U ion signal intensities (Fig. 15-7a) with the decay (+ washout) times averaging ~15 seconds. Decay times for ablation runs of zircon standards BR266 (Stern & Amelin 2003) and 91500 (Wiedenbeck *et al*. 1995) using the standard laser ablation cell also yielded comparable decay (+ washout) times of ~15 seconds; this despite the fact that 3 to 10 times more ^{238}U ion signal (*i.e.*, >0.2 volts) was recorded during the ablation of BR266 using a 40 μm spot size (Fig. 15-7). Decay (+ washout) patterns for the ^{206}Pb ion signals measured on IC1 were also similar for both types of ablation cells and accomplished in <10 seconds (Fig. 15-7b); thus a little faster than that observed for ^{238}U (Fig. 15-7a). Thus, the results shown in Fig. 15-7 indicate that both types of laser ablation cells are characterized by similar washout times. Moreover, 15 seconds is much shorter than the total amount of time taken in between consecutive zircon analyses (~1 minute). The latter is the time required to displace the cell to the position of the subsequent

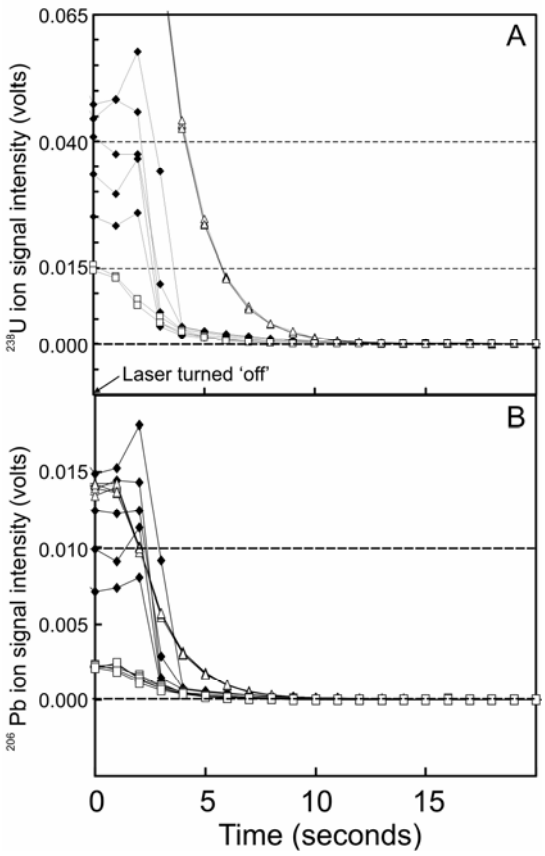

FIG. 15-7. Diagram illustrates the variation in ^{238}U (**A**) and ^{206}Pb (**B**) ion signals *versus* time (seconds) measured on Faraday bucket EX-H and electron multiplier IC1, respectively, subsequent to switching 'off' the laser unit following the completion of a 30-second ablation analysis of various zircon standards. Filled diamonds = ablation runs of internal zircon standard LH94-15 using the SuperCell™; Open triangles = ablation runs of international zircon standard BR266 using the standard cell; Open squares = ablation runs of international zircon standard 91500 using the standard cell.

grain to be analyzed and precisely locate the analysis spot within the grain with the aid of either back-scattered electron or cathodoluminescent images.

The 'sensitivity' or ion signal yield was also investigated for both the standard ablation cassette and SuperCell™ with repeated measurements of zircon standard BR266 analyzed using identical instrument conditions. Despite having conducted the tests during different analytical sessions, any bias with regards to differing sensitivity resulting from other instrument parameters (*e.g.*, cones, quartz torch assembly) is eliminated by normalization of the ^{238}U and ^{206}Pb to equivalent ^{205}Tl ion signals (Fig. 15-8). The latter is introduced via the desolvating nebuliser (DSN-100) in solution mode and thus independent of the laser ablation conditions. The laser ablation results shown in Fig. 15-8 indicate that the SuperCell™ yields slightly higher ion signals for both Pb and U compared to the standard cell. However, compared to the standard cell laser ablation runs, the analyses conducted with the SuperCell are characterized by slightly less stable ion signals, in particular during the last 5 seconds of analysis (Fig. 15-8). Despite this feature, the results from the laser ablation runs obtained with the SuperCell™ in general yield measured Pb/Pb and Pb/U values with similar internal precision relative to those obtained with the standard cell (examples provided in 'Results' section below). Given the overall similarity in performances relative to ion signal yield and ion signal decay (+washout) times for the standard and SuperCell™ cassettes, both were utilized in conducting the laser ablation analysis of unknown accessory minerals within petrographic thin sections.

Petrographic examination, measurement protocol and data reduction

Prior to any analytical session, the petrographic thin sections to be investigated are carefully examined. This serves both to locate the accessory minerals and evaluate the paragenesis of the grains in the context of deformational fabrics and other salient features in the section. Petrographic examination is typically followed by backscattered

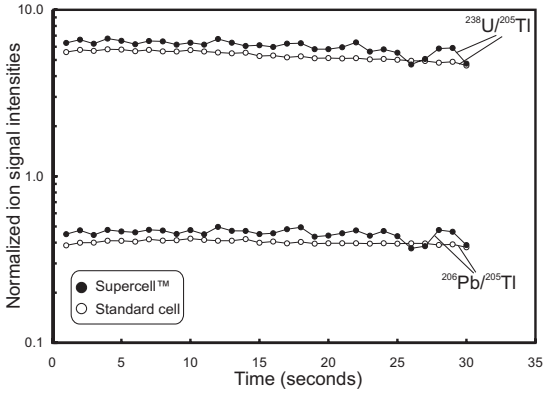

FIG. 15-8. A plot of log $^{206}Pb/^{205}Tl$ and $^{238}U/^{205}Tl$ values *versus* time (seconds) for ablation runs of BR266 (*i.e.*, same epoxy mount) using both the standard ablation cell and SuperCell™ and identical instrument conditions. The curves represent average values of three individual measurements.

electron imaging of the selected grains by electron microprobe. This step highlights compositional zonation or metamict areas within the grains and thereby enables optimal citing of spots for isotopic analysis. The carbon coat required for BSE imaging is subsequently removed and areas containing accessory minerals to be analyzed are circled with a marker pen (Fig. 15-9).

The following description of the LA–MC–ICP–MS analytical protocol is summarized from more detailed descriptions in Simonetti *et al*. (2005, 2006). At the start of each analytical session, the Faraday-ion counter bias is determined using a mixed 0.4 ppb standard solution of Pb (NIST SRM 981) and Tl (NIST SRM 997). The Faraday-multiplier calibration is calculated using a two sequence acquisition cycle, where the $^{207}Pb/^{206}Pb$ (= 0.914585; Todt *et al*. 1996) is measured on the IC1 (ion counter #1)–L3 (Faraday) combination. The IC0 (ion counter #0) and IC2 (ion counter #2) calibrations are determined against the IC1 bias using the measured $^{207}Pb/^{206}Pb$ and $^{206}Pb/^{204}Pb$ (=16.9356; Todt *et al*. 1996) values, respectively. This approach is similar to that adopted in previous isotopic studies involving MC–ICP–MS instruments equipped with multiple ion-counting devices (Taylor *et al*. 2003). A routine U–Pb analysis consists of a 30 second blank measurement (He + Ar gases + 2%HNO_3 acid) prior to the commencement of the laser ablation. Background levels of ^{206}Pb and ^{207}Pb are typically less than 200 cps each, and the combined $^{204}Pb+^{204}Hg$ background ion signal is generally <1000 cps; these background ion signal intensities are extremely stable and reproducible during the course of an analytical session. The ablated particles are transported into the sample-out line (Saint-Gobain Tygon® tubing) with a He carrier gas and mixed with nebulized Tl via a 'Y'-connection located just prior to the torch box. The simultaneous introduction of laser-induced and dried solution aerosols was developed several years ago as an alternative calibration method for various laser ablation-ICP–MS instruments (*e.g.*, Chenery & Cook 1993, Günther *et al*. 1997). A NIST SRM 997 Tl isotopic standard solution (1 ppb in 2% HNO_3) is nebulized using a DSN-100 desolvating introduction system (Nu Instruments, UK) and aspirated (free aspiration mode) into the

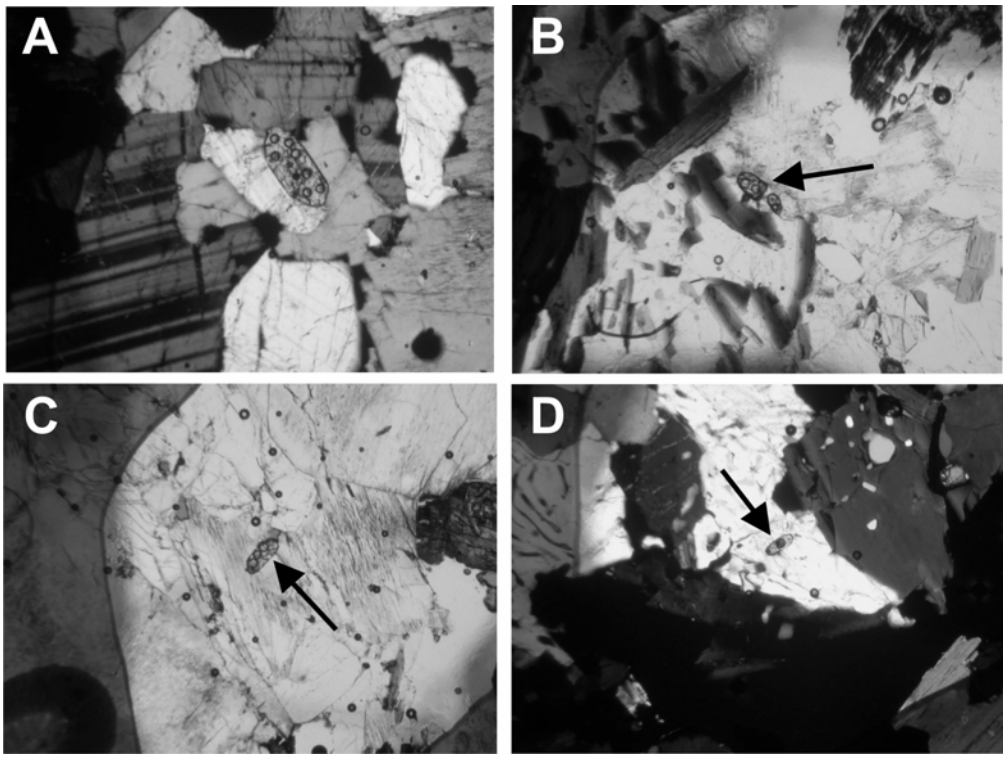

FIG. 15-9. Photomicrographs of areas delineated with a blue marker pen containing zircon in petrographic thin section of sample 243-336E (see main text for petrographic description). The zircon grains contain laser ablation pits of 40 μm in diameter and the corresponding U–Pb isotope data are shown in Figure 15-11 and listed in Table 15-3 for zircon grains labeled #1 (**A**), #2 (**B**), #3 (**C**), and #4 (**D**). Please note that zircon #2 (B) and #4 (D) indicate inherited ages of *ca*. 2.5 Ga.

ICP source during the laser ablation run. Both the spray chamber and desolvating membrane of the DSN-100 are heated to 110ºC, with the Ar (Argon) flow rate set to 0.3 L min^{-1} and 2.7–3.2 L min^{-1} for the spray chamber and desolvating membrane, respectively. The measured Pb/U values are positively correlated with the membrane gas flow rate (Simonetti *et al*. 2005), and this is an expected result since varying the mixture of He and Ar within the main sample-out tube will most certainly change the plasma characteristics (*e.g.*, Eggins *et al*. 1998, Horn *et al*. 2000). The measured $^{205}Tl/^{203}Tl$ value is used to correct the measured Pb isotope ratios for instrumental mass bias using the reference value of 2.3871 (Dunstan 1980). The analytical protocol adopted here involving a Tl-doping method for monitoring of instrumental mass bias yields 2σ relative standard deviations that are 0.3 to 1% ($^{207}Pb/^{206}Pb$) and 1 to 3% ($^{206}Pb/^{238}U$ and $^{207}Pb/^{235}U$). Figure 15-10 illustrates the average and typical external reproducibility (2σ level) obtained for the $^{207}Pb/^{206}Pb$ ratio during repeated measurement of the in-house external zircon standard LH94-15 (described below) using the Tl-doped protocol described here during an analytical session. Simonetti *et al*. (2005) investigated the external reproducibility for both Tl-doped and non-Tl-doped (*i.e.*, mass bias controlled solely by external matrix-matched standard) methods and these yielded 0.5% to 0.34% (2σ level), respectively; this is entirely in agreement with the external reproducibility (0.32%; 2σ level) obtained for the analyses shown in Fig. 15-10. Moreover, the average $^{207}Pb/^{206}Pb$ of 0.11191 ± 0.00036 shown in Fig. 15-10 is within uncertainty to the ID–TIMS value (0.111869; Ashton *et al*. 1999) and validates the analytical method employed here.

Correction for LIEF (laser induced element fractionation) during a single laser ablation session of unknowns using the Tl-doping method was achieved by analysis of the matrix-matched 'external' standards of zircon (BR266 – Stern & Amelin 2003; 91500 – Wiedenbeck *et al*. 1995; LH94–15 – Ashton *et al*. 1999), and monazite (Western Australia and Madagascar – Heaman *et al*., unpublished ID–TIMS data). The measured Pb/U values for the unknowns are compared to those obtained for their respective standards (ablated using identical run conditions) at the start of an analytical session, and normalization (= measured value/'true' value) factors are determined. Analytical uncertainties associated with the $^{207}Pb/^{206}Pb$ and Pb/U values for individual analyses were propagated relative to the external reproducibility obtained for the external zircon standard and followed the procedure outlined in Horstwood *et al*. (2003). Subsequent to the study by Simonetti *et al*. (2006), the uncertainty associated with the common Pb correction based on the calculation of the absolute count rate of ^{204}Pb (cps; Simonetti *et al*. 2005) is propagated as part of the total error associated with the $^{207}Pb/^{206}Pb$ values. This error propagation is significant primarily when accessory minerals are characterized by a high amount of common Pb, or yield relatively low Pb ion signals (*e.g.*, young zircon <200 Ma old). A more detailed discussion of the error propagation associated with the common Pb correction is given in Horstwood *et al*. (2008). As outlined in Simonetti *et al*. (2005), the true amount of common ^{204}Pb

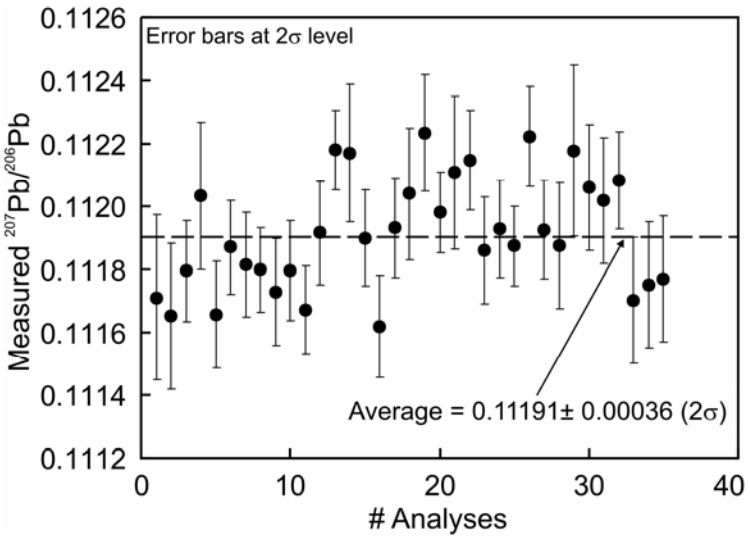

FIG. 15-10. Plot of measured $^{207}Pb/^{206}Pb$ *versus* analysis number (n= 35) for repeated laser ablation measurements of the in-house LH94-15 zircon standard during a single analytical session (~9 hours) using the Tl-doped method to monitor instrumental mass bias. The average $^{207}Pb/^{206}Pb$ value of 0.11191 ± 0.00036 (2σ) is indistinguishable compared to the accepted ID–TIMS value of 0.111869 ± 0.00006 (2σ; Ashton *et al*. 1999).

present within the zircon (or monazite) as opposed to ^{204}Hg possibly produced during the ablation process is evaluated off-line by graphical means using a plot of total 204 ion signal intensity *versus* the measured ^{207}Pb/^{206}Pb ratio. In theory, if the 204 ion signal is derived entirely from common Pb *intrinsic* to the zircon, then one should obtain a horizontal line on such a plot. A negative correlation between the total 204 ion signal and measured ^{207}Pb/^{206}Pb diagram most likely indicates the presence of ^{204}Hg produced during the ablation process (unless of course a common Pb-bearing mineral inclusion was ablated during the analysis). In the case of the latter situation, the true amount of ^{204}Pb intrinsic to the mineral is taken to be zero.

The data presented in the 'Results' section have been obtained using all of the calibration procedures and data reduction protocols outlined in this paper and those described in Simonetti *et al*. (2005, 2006). The correlation coefficients ('rho' values) for the Pb/U ratios were calculated according to the equations defined in Ludwig (2003).

RESULTS

Background

U–Pb geochronology of uranium-bearing accessory minerals is based on the radioactive decay schemes of the two unstable uranium nuclides, ^{238}U (decay constant = 1.55125 x 10^{-10} yr^{-1}) and ^{235}U (decay constant = 9.8485 x 10^{-10} yr^{-1}; both constants from Jaffey *et al*., 1971); these decay through a series of intermediate daughter products to the stable daughter isotopes of ^{206}Pb and ^{207}Pb, respectively. Thus, two independent apparent ages (dates) can be obtained from each geochronometer, *i.e.*, ^{206}Pb/^{238}U and ^{207}Pb/^{235}U, for every isotopic analysis of a U-bearing accessory mineral (*e.g.*, zircon, monazite, titanite, baddeleyite, perovskite). If the mineral being analyzed has remained 'closed' with regards to either gain or loss of parent and/or daughter isotopes since its time of formation, then the two Pb/U chronometers shall yield identical ages. This is then referred to as a 'concordant' analysis or age. A plot of ^{206}Pb/^{238}U *vs*. ^{207}Pb/^{235}U is referred to as a 'concordia' diagram and illustrates the 'concordia' curve; the latter represents the locus of identical or '*concordant*' Pb/U ages throughout geologic time (*e.g.*, Fig. 15-11). Analyses of accessory minerals that have undergone gain or loss of either Pb and/or U typically do not yield concordant analyses (*i.e.*, plot on the concordia curve) but rather define colinear arrays on the

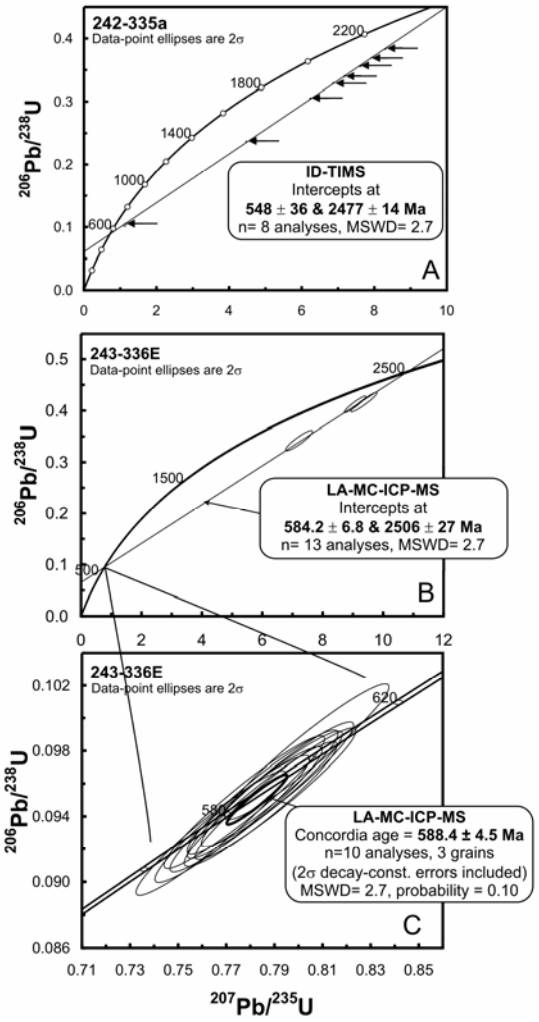

FIG. 15-11. Concordia plots that contain the U–Pb age results for (**A**) sample 242-335A (ID–TIMS results) with arrows indicating position of individual analyses (Table 15-3); (**B**) sample 243-336E obtained by LA–MC–ICP–MS; and (**C**) enlarged view of lower intercept region from plot shown in B. These concordia plots and those shown in subsequent diagrams were constructed with Isoplot version 3.00 (Ludwig 2003).

concordia plot; these analyses are referred to as '*discordant*' and the best-fit line through these data is called a '*discordia*' or mixing line (*e.g.*, Fig. 15-11a, b). Both the upper and lower intercepts between the discordia line and the concordia curve are interpreted to represent ages of geological events, such as time of magma emplacement and much later metamorphic event (*e.g.*, Fig. 15-11a, b). In subsequent sections, several ages or dates are also reported as '*weighted mean*' ^{207}Pb/^{206}Pb or ^{206}Pb/^{238}U ages as calculated by Isoplot version 3.0

(Ludwig, 2003); this algorithm takes into account the scatter (MSWD – mean square weighted deviation). If the latter is not much greater than 1, then the weighted mean is determined by weighting each data point by its inverse variance and associated uncertainty. In contrast, a 'concordia age' is the most probable age for an analysis (or weighted mean) on a concordia diagram, where the true location of the analysis is assumed to fall precisely on the concordia curve (Ludwig, 2003).

Zircon – Cardamom Hills Massif, southern India

Samples 243-336E and 247-339C are from the 'Cardamom Hills' massif, one of the large charnockite massifs of the southern Indian granulite terrain. The massif is characterized by at least three different types of charnockite that formed at different times and have variable major- and trace-element compositions.

Sample 243-336E is a late stage felsic dyke that clearly cross-cuts the foliation in one of the charnockite/enderbite units. The dyke is coarse grained and consists of perthitic alkali feldspar, quartz, subordinate plagioclase, biotite and retrogressed orthopyroxene. Accessory minerals include coarse grained zircon and abundant Th-rich, U-poor monazite. The U–Pb ID–TIMS results for eight small multi-grain and single zircon grains (Table 15-3) in a broadly similar charnockite (242-335A) from nearby outcrops define a discordia line that is interpreted to indicate that the rocks which host the dyke formed at *ca*. 2.5 Ga and experienced a Pan-African overprint at *ca*. 550 Ma (Fig. 15-11a).

A petrographic thin section of sample 243-336E was analyzed using the standard laser ablation cell and the Pb/U LIEF was monitored and bracketed by repeated analysis of the in-house zircon standard LH94-15 (Ashton *et al*. 1999; Fig. 15-2). The LA–MC–ICP–MS U–Pb dating results for 4 zircon grains analyzed at 40 micrometres spatial resolution are listed in Table 15-3 and shown in Fig. 15-11b. These four analyses plot along an identical mixing line with overlapping upper and lower intercept ages compared to the ID–TIMS data for charnockite 242-335A (Fig. 15-11a). In addition, 10 analyses from three zircon grains in sample 243-336E yielded a precise concordant age of 588.4 ± 4.5 Ma (2σ; Fig. 15-11c), which we interpret to be the crystallization age of the felsic dyke.

Sample 247-339C is a very coarse grained patch or pod (partial melt?) hosted within the finer grained charnockite. It comprises alkali feldspar, quartz, and plagioclase along with large grains of orthopyroxene, which in some cases have rims of hornblende; accessory minerals include apatite, Fe-Ti oxides and zircon. U–Pb ID–TIMS analysis of three zircon fractions from a nearby charnockite of similar major- and trace-element composition (188-281a, b) to the host charnockite of sample 247-339C yielded a discordia line with an upper intercept ~820 Ma and a lower intercept ~520 Ma (Table 15-3; Fig. 15-12a).

A petrographic thin section of sample 247-339C was analyzed using the SuperCell™ laser ablation cassette. As mentioned earlier, one advantage of this cell compared to the standard ablation cassette is the capacity to house zircon standards mounted on glass slides simultaneously and placed adjacent to the thin section to be analyzed (in the central area). The Pb–U 'LIEF' was monitored by intermittent analysis of the in-house zircon standard LH94-15 grains mounted on a glass slide (~0.5 cm x ~0.5 cm). The LA–MC–ICP–MS results for 17 analyses of 6 zircon grains

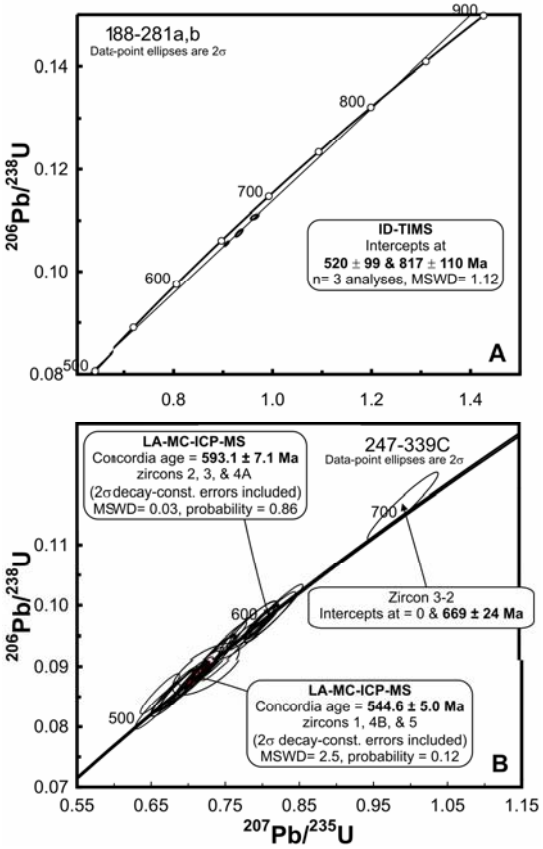

FIG. 15-12. Concordia plots illustrating the U–Pb age results for (A) sample 188-281a, b (by ID–TIMS); (B) LA–MC–ICP–MS results for sample 247-339C.

TABLE 15-3. U-PB RESULTS FOR ZIRCON AND MONAZITE

Anal.#	Spot size (μm)	^{206}Pb cps	^{206}Pb/^{204}Pb	^{207}Pb/^{206}Pb	2σ uncert.	^{207}Pb/^{235}U	2σ uncert.	^{206}Pb/^{238}U	2σ uncert.	'rho'	^{207}Pb/^{206}Pb Age (Ma)	^{207}Pb/^{206}Pb 2σ uncert.	^{206}Pb/^{238}U Age (Ma)	^{206}Pb/^{238}U 2σ uncert.	% Disc.
243-336E															
zircon 4-1	40	167683	3422	0.16321	0.00194	9.3659	0.3556	0.4164	0.0156	0.950	2489	±20	2244	±84	9.8
zircon 2-2	40	544941	16513	0.15951	0.00174	9.0678	0.2942	0.4121	0.0133	0.943	2450	±18	2225	±72	9.2
zircon 2-1	40	327641	7446	0.15345	0.00320	7.2177	0.3653	0.3420	0.0161	0.912	2385	±35	1896	±89	20.5
zircon 1-1	40	294897	infinite	0.06001	0.00063	0.7861	0.0263	0.0953	0.0032	0.951	604	±23	587	±20	2.8
zircon 1-2	40	280451	infinite	0.05969	0.00063	0.7782	0.0259	0.0944	0.0031	0.950	592	±23	582	±19	1.8
zircon 1-3	40	442333	infinite	0.05942	0.00063	0.7775	0.0273	0.0949	0.0033	0.954	583	±23	584	±20	-0.3
zircon 1-4	40	482446	infinite	0.05947	0.00062	0.7637	0.0255	0.0930	0.0031	0.952	584	±22	573	±19	1.9
zircon 1-5	40	394251	infinite	0.05986	0.00064	0.7913	0.0259	0.0959	0.0031	0.947	598	±23	591	±19	1.3
zircon 1-6	40	389059	infinite	0.05969	0.00063	0.7851	0.0256	0.0955	0.0031	0.948	592	±23	588	±19	0.8
zircon 1-7	40	291868	infinite	0.05983	0.00065	0.7843	0.0260	0.0947	0.0031	0.947	598	±23	584	±19	2.3
zircon 3-1	40	553897	infinite	0.05957	0.00062	0.8034	0.0280	0.0979	0.0034	0.955	588	±23	602	±21	-2.5
zircon 3-2	40	455179	infinite	0.05976	0.00062	0.7905	0.0273	0.0954	0.0033	0.955	595	±22	587	±20	1.3
zircon 3-3	40	307897	infinite	0.05972	0.00064	0.7725	0.0263	0.0938	0.0032	0.950	594	±23	578	±20	2.6
247-339C															
zircon 2-1	40	230297	infinite	0.06024	0.00067	0.8138	0.0284	0.0981	0.0034	0.949	612	±24	603	±21	1.5
zircon 2-2	40	193247	32208	0.05956	0.00079	0.7893	0.0274	0.0967	0.0032	0.924	588	±29	595	±20	-1.3
zircon 3-1	40	226262	infinite	0.06036	0.00069	0.8190	0.0321	0.0988	0.0038	0.958	616	±25	607	±24	1.5
zircon 4A-1	40	182137	18214	0.05939	0.00106	0.7845	0.0333	0.0960	0.0038	0.908	581	±39	591	±23	-1.6
zircon 4A-2	40	1005883	infinite	0.05961	0.00062	0.7571	0.0317	0.0925	0.0039	0.969	590	±22	570	±24	3.3
zircon 4B-1	40	808141	infinite	0.05852	0.00060	0.7356	0.0262	0.0913	0.0032	0.959	549	±22	563	±20	-2.6
zircon 4B-2	40	899776	449888	0.05845	0.00059	0.7440	0.0316	0.0925	0.0039	0.971	547	±22	570	±24	-4.3
zircon 4B-3	40	942588	188518	0.05852	0.00060	0.7303	0.0288	0.0906	0.0036	0.966	549	±22	559	±22	-1.8
zircon 4B-4	40	507954	126988	0.05840	0.00061	0.7068	0.0247	0.0879	0.0031	0.955	545	±23	543	±19	0.4
zircon 5-1	40	113735	28434	0.05789	0.00084	0.6822	0.0265	0.0856	0.0032	0.928	526	±32	530	±20	-0.8
zircon 5-2	40	139044	infinite	0.05886	0.00072	0.7371	0.0254	0.0913	0.0031	0.936	562	±27	563	±19	-0.2
zircon 1-1	40	167479	infinite	0.05833	0.00065	0.6936	0.0264	0.0871	0.0033	0.956	542	±25	538	±20	0.7
zircon 1-2	40	165637	infinite	0.05797	0.00067	0.7159	0.0285	0.0890	0.0035	0.958	528	±25	549	±22	-4.0
zircon 1-3	40	121963	infinite	0.05785	0.00067	0.6893	0.0250	0.0864	0.0031	0.949	524	±25	534	±19	-1.9
zircon 1-4	40	172343	infinite	0.05850	0.00067	0.7158	0.0243	0.0890	0.0030	0.942	548	±25	549	±18	-0.2
zircon 3-2	40	864436	9196	0.06209	0.00072	0.9932	0.0390	0.1164	0.0045	0.956	677	±25	710	±28	-4.9
242-335A (TIMS)															
1z, col. abr.				0.07935	0.00194	1.13100	0.0312	0.10337	0.0021	0.508	1181	±48	634	13	46.3
2z, col. abr.				0.13677	0.00018	4.46800	0.0138	0.23693	0.0007	0.905	2187	±2	1371	4	37.3
3z, col. abr.				0.15529	0.00024	7.62443	0.0242	0.35610	0.0011	0.876	2405	±3	1964	6	18.4
4z, col. abr.				0.15552	0.00011	7.91027	0.0231	0.36890	0.0011	0.973	2408	±1	2024	6	15.9
5z, col. abr.				0.15725	0.00012	8.31274	0.0238	0.38340	0.0011	0.964	2426	±1	2092	6	13.8
6z, col. abr.				0.15321	0.00033	7.18704	0.0277	0.34023	0.0012	0.827	2382	±4	1888	6	20.8
7z, col. abr.				0.51270	0.00032	6.86820	0.0191	0.32929	0.0009	0.975	4278	±1	1835	5	57.1
8z, col. abr.				0.14804	0.00012	6.23494	0.0173	0.30546	0.0009	0.959	2323	±1	1718	5	26.0
1z, col. abr.				0.07935	0.00194	1.13100	0.0312	0.10337	0.0021	0.508	1181	±48	634	13	46.3

TABLE 15-3 (CONTINUED). U-PB RESULTS FOR ZIRCON AND MONAZITE

Anal.#	Spot size (μm)	^{206}Pb cps	^{206}Pb/ ^{204}Pb	^{207}Pb/ ^{206}Pb	2σ uncert.	^{207}Pb/ ^{235}U	2σ uncert.	^{206}Pb/ ^{238}U	2σ uncert.	'rho'	^{207}Pb/^{206}Pb Age (Ma)	2σ uncert.	^{206}Pb/^{238}U Age (Ma)	2σ uncert.	% Disc.
188-281a (TIMS)															
1z, lt. pink				0.06314	0.00032	0.9640	0.0064	0.1107	0.0004	0.63	713	±11	677	3	5.0
2z, col.				0.06235	0.00013	0.9074	0.0041	0.1055	0.0004	0.882	686	±5	647	3	5.7
188-281b (TIMS)															
1z, col abr				0.06283	0.00023	0.9323	0.006	0.1076	0.0006	0.824	702	±8	659	4	6.2
GJ1-32 (Fig. 15-10)															
1	40	429248	28617	0.06040	0.00082	0.8253	0.0326	0.0992	0.0038	0.939	618	±29	610	±23	1.4
2	40	456445	infinite	0.06040	0.00065	0.8209	0.0349	0.0983	0.0042	0.968	618	±23	604	±26	2.2
3	40	458752	24145	0.05964	0.00089	0.8214	0.0311	0.1000	0.0036	0.920	590	±32	614	±22	-4.0
4	40	495851	infinite	0.06048	0.00062	0.8314	0.0320	0.1003	0.0039	0.965	621	±22	616	±24	0.7
5	40	482876	infinite	0.06015	0.00063	0.8338	0.0281	0.1006	0.0034	0.952	609	±23	618	±21	-1.5
6	40	408628	58375	0.06016	0.00067	0.8026	0.0303	0.0967	0.0036	0.956	609	±24	595	±22	2.3
7	40	436632	33587	0.05976	0.00077	0.7795	0.0306	0.0942	0.0036	0.945	595	±28	580	±22	2.4
9	40	368644	infinite	0.06033	0.00063	0.8012	0.0283	0.0965	0.0034	0.957	615	±22	594	±21	3.5
11	40	426769	47419	0.05988	0.00070	0.7930	0.0298	0.0961	0.0036	0.951	599	±25	592	±22	1.3
12	40	443445	88689	0.06023	0.00064	0.7992	0.0291	0.0963	0.0035	0.957	612	±23	593	±21	3.1
14	40	394255	49282	0.05991	0.00069	0.7916	0.0282	0.0958	0.0034	0.947	600	±25	590	±21	1.8
15	40	360321	45040	0.06002	0.00071	0.7881	0.0263	0.0951	0.0031	0.936	604	±26	586	±19	3.1
GJ1-32 Fig. 15-11b)															
1	40	434524	108631	0.06017	0.00063	0.7995	0.0311	0.0965	0.0037	0.963	610	±23	594	±23	2.6
2	40	440443	infinite	0.06020	0.00062	0.7856	0.0262	0.0948	0.0032	0.952	611	±22	584	±19	4.4
3	40	418573	41857	0.05988	0.00072	0.7722	0.0272	0.0937	0.0032	0.941	599	±26	577	±20	3.7
4	40	442918	infinite	0.06021	0.00063	0.8251	0.0303	0.0994	0.0036	0.960	611	±22	611	±22	0.0
5	40	443444	infinite	0.06026	0.00063	0.8139	0.0320	0.0980	0.0038	0.965	613	±22	603	±24	1.7
6	40	444410	24689	0.05987	0.00088	0.8201	0.0269	0.0995	0.0031	0.896	599	±32	612	±19	-2.1
7	40	446688	infinite	0.06002	0.00062	0.7988	0.0253	0.0965	0.0030	0.946	604	±23	594	±19	1.7
8	40	437755	54719	0.06014	0.00068	0.8062	0.0272	0.0973	0.0032	0.943	609	±24	599	±20	1.7
9	40	460438	infinite	0.05998	0.00063	0.8032	0.0262	0.0972	0.0032	0.948	603	±23	598	±19	0.8
10	40	461895	230948	0.06017	0.00062	0.8254	0.0269	0.0996	0.0032	0.950	610	±22	612	±20	-0.4
11	40	450208	225104	0.06009	0.00062	0.8072	0.0258	0.0978	0.0031	0.947	607	±22	602	±19	0.9

TABLE 15-3 (CONTINUED). U-PB RESULTS FOR ZIRCON AND MONAZITE

Anal.#	Spot size (μm)	^{206}Pb cps	^{206}Pb/^{204}Pb	^{207}Pb/^{206}Pb	2σ uncert.	^{207}Pb/^{235}U	2σ uncert.	^{206}Pb/^{238}U	2σ uncert.	'rho'	^{207}Pb/^{206}Pb Age (Ma)	2σ uncert	^{206}Pb/^{238}U Age (Ma)	2σ uncert	% Disc
LH98-239															
zircon 1-1	40	132724	infinite	0.08520	0.00092	2.7099	0.1297	0.2310	0.0110	0.974	1320	±21	1340	±64	-1.5
zircon 2-1	40	152020	infinite	0.08437	0.00093	2.6198	0.0942	0.2243	0.0080	0.952	1301	±22	1304	±46	-0.2
zircon 2-2	40	150613	infinite	0.08425	0.00088	2.6076	0.1046	0.2249	0.0090	0.966	1298	±20	1308	±52	-0.7
zircon 3-1	40	311900	infinite	0.08437	0.00090	2.5980	0.0943	0.2237	0.0081	0.957	1301	±21	1301	±47	0.0
zircon 3-2	40	355591	infinite	0.08388	0.00087	2.5326	0.0931	0.2192	0.0080	0.960	1290	±20	1278	±47	0.9
zircon 4-2	40	55005	infinite	0.08353	0.00098	2.5948	0.0978	0.2253	0.0084	0.951	1282	±23	1310	±49	-2.2
zircon 4-b1	40	189233	infinite	0.08436	0.00090	2.6223	0.1065	0.2259	0.0091	0.966	1301	±21	1313	±53	-0.9
zircon 5-1	40	57627	infinite	0.08500	0.00126	2.5781	0.1032	0.2204	0.0085	0.930	1316	±29	1284	±49	2.4
zircon 5-2	40	269343	7696	0.08443	0.00121	2.6280	0.1084	0.2258	0.0076	0.914	1302	±28	1312	±44	-0.8
zircon 5-3	40	203445	infinite	0.08474	0.00090	2.6903	0.0930	0.2308	0.0079	0.953	1310	±21	1339	±46	-2.2
zircon 6-2	40	92428	infinite	0.08449	0.00096	2.6547	0.1063	0.2272	0.0090	0.960	1304	±22	1320	±52	-1.2
zircon 6-3	40	90320	infinite	0.08482	0.00095	2.6519	0.0980	0.2259	0.0083	0.954	1311	±22	1313	±48	-0.1
zircon 7-1	40	210122	infinite	0.08485	0.00091	2.6601	0.0891	0.2276	0.0076	0.948	1312	±21	1322	±44	-0.8
zircon 7-2	40	100709	infinite	0.08491	0.00100	2.6143	0.0891	0.2192	0.0073	0.940	1313	±23	1278	±43	2.7
zircon 1-2	40	1392378	infinite	0.08379	0.00086	2.7149	0.1282	0.2356	0.0111	0.976	1288	±20	1364	±64	-5.9
zircon 4b-2	40	109384	infinite	0.08471	0.00096	2.7833	0.0961	0.2369	0.0081	0.945	1309	±22	1371	±47	-4.7
zircon 6-1	40	223788	infinite	0.08463	0.00090	2.7376	0.1027	0.2346	0.0088	0.959	1307	±21	1359	±51	-4.0
zircon 4-1	40	536435	infinite	0.08440	0.00092	2.7180	0.1105	0.2339	0.0095	0.964	1302	±21	1355	±55	-4.1
LH98-239 (TIMS)															
1			3998	0.08468	0.00014	2.5929	0.0108	0.2221	0.0008	0.918	1308.1	±3	1292.9	±4	1.3
2			15571	0.08445	0.00012	2.5814	0.0102	0.2217	0.0008	0.925	1302.9	±3	1290.9	±4	1.0
ST-3a-mnz															
Grain 1-4	12	1117737	infinite	0.15309	0.00157	8.9391	0.27	0.42358	0.016	0.977	2381	±17	2279	±71	5.2
Grain 1-5	12	2016729	infinite	0.15424	0.00155	9.3149	0.28	0.43821	0.014	0.954	2394	±17	2345	±65	2.5
Grain 1-6	12	1728835	infinite	0.15329	0.00154	9.2486	0.28	0.43787	0.016	0.967	2383	±17	2343	±70	2.1
Grain 1-7	12	1722542	infinite	0.15336	0.00154	9.2437	0.28	0.43744	0.015	0.963	2384	±17	2341	±68	2.2
Grain 1-9	12	1350243	infinite	0.15331	0.00155	9.4298	0.28	0.44623	0.015	0.953	2383	±17	2380	±65	0.2
Grain 2-3	12	1262285	infinite	0.15315	0.00159	9.1431	0.27	0.43313	0.020	0.652	2381	±18	2322	±89	3.1
Grain 2-4	12	1546549	infinite	0.15272	0.00154	9.2401	0.28	0.43878	0.014	0.947	2377	±17	2347	±62	1.6
Grain 3-4	12	1998724	infinite	0.16114	0.00165	10.0697	0.30	0.45327	0.015	0.953	2468	±17	2412	±67	2.8
Grain 3-6	12	1800729	infinite	0.16254	0.00166	10.3013	0.31	0.45956	0.014	0.945	2482	±17	2440	±63	2.2
Grain 3-7	12	2284983	infinite	0.16162	0.00167	10.2972	0.31	0.46196	0.014	0.942	2473	±17	2450	±63	1.2
Grain 3-9	12	1385241	infinite	0.15328	0.00156	9.2990	0.28	0.44015	0.014	0.945	2383	±17	2353	±61	1.6
Grain 3-10	12	1280531	infinite	0.15320	0.00156	9.4299	0.28	0.44662	0.018	0.737	2382	±17	2382	±81	0.1
Grain 4-4	12	1422891	infinite	0.16259	0.00167	10.2183	0.31	0.45653	0.014	0.946	2483	±17	2426	±64	2.8
Grain 4-5	12	1402247	infinite	0.16353	0.00166	10.3015	0.31	0.45680	0.016	0.958	2492	±17	2427	±69	3.2
Grain 4-6	12	1320995	infinite	0.16294	0.00165	10.0907	0.30	0.44803	0.014	0.948	2486	±17	2388	±63	4.8
Grain 4-7	12	1627700	infinite	0.15430	0.00159	8.9641	0.27	0.42149	0.015	0.959	2394	±18	2269	±66	6.3

within one petrographic thin section of sample 247-339C are listed in Table 15-3 and shown in Fig. 15-12b. The data can be separated into three distinct age groups: zircon samples 1, 4B and 5 define the youngest concordant age at 544.6 ±5.0 Ma (2σ), whereas zircon samples 2, 3, and 4A yield a concordant age at 598.1 ±8.0 Ma (2σ); the core analysis (3-2) of zircon #3 yields an inherited age of 669 ±24 Ma (2σ). Anchoring the ID–TIMS data for sample 188-281a, b to the more precise lower intercept age of 544.6 ± 5 Ma obtained by LA–MC–ICP–MS yields an upper intercept age of 850 ± 20 Ma. This upper intercept date most probably represents the magma crystallization age of the host charnockite or its granitoid protolith. The 544.6 ± 5.0 Ma date represents the time at which the coarse grained melt patch/pod formed, and the 598.1 ± 8 Ma and *ca*. 670 Ma age populations most probably reflect the ages of zircon inherited from the host charnockite. Of interest, the *ca*. 590 Ma age component in the host charnockite determined at this location was also documented in a previous geochronological study conducted on this charnockite massif (Miller *et al*., 1996). Thus, combining the laser ablation and ID–TIMS data, there is evidence for four major events in the Cardamom massif at *ca*. 2500 Ma, 850 Ma, 590 Ma and 545 Ma.

During the same analytical session, a second glass mount (~0.5 cm x ~0.5 cm) containing zircon fragments from aliquot GJ-1-32 (obtained from Macquarie University) was placed adjacent to the mount bearing the LH94-15 grains. Eight ID–TIMS analyses of four separate GJ-1-32 fragments by F. Corfu (University of Oslo) yielded a weighted mean $^{207}Pb/^{206}Pb$ age of 608.53 ±0.37 Ma (2σ; Jackson *et al*. 2004). ID–TIMS analysis of five GJ-1-32 zircon fragments conducted at the University of Alberta yield a weighted mean $^{207}Pb/^{206}Pb$ age of 606.7 ±2.3 Ma (2σ). Repeated laser ablation analysis (n=12) of GJ1-32 zircon grains using a 40 micrometre spot size yielded a weighted mean $^{207}Pb/^{206}Pb$ age of 608.8 ± 7.0 Ma (2σ; Fig. 15-13). The ID–TIMS and LA–MC–ICP–MS ages obtained in this study are indistinguishable within their associated uncertainties, and also overlap the ID–TIMS age for GJ–1 zircon reported by Jackson *et al*. (2004).

Zircon: Voisey's Bay Granite. Sample LH98-239 is a medium grained clinopyroxene-fayalite granite from the Voisey's Bay intrusion, Labrador. In decreasing abundance, it consists of perthitic alkali feldspar, plagioclase, quartz, amphibole, clinopyroxene, fayalitic olivine and ulvospinel with subordinate zircon, pyrite, apatite and secondary biotite. Clinopyroxene and olivine typically form irregular clusters commonly surrounded by amphibole. Zircon is an abundant accessory mineral in this sample, has high Th/U (0.79), and forms relatively large euhedral oscillatory zoned crystals intergrown with a variety of minerals.

ID–TIMS analyses were conducted at the University of Alberta on two small multi-grain zircon fractions from sample LH98-239 and these

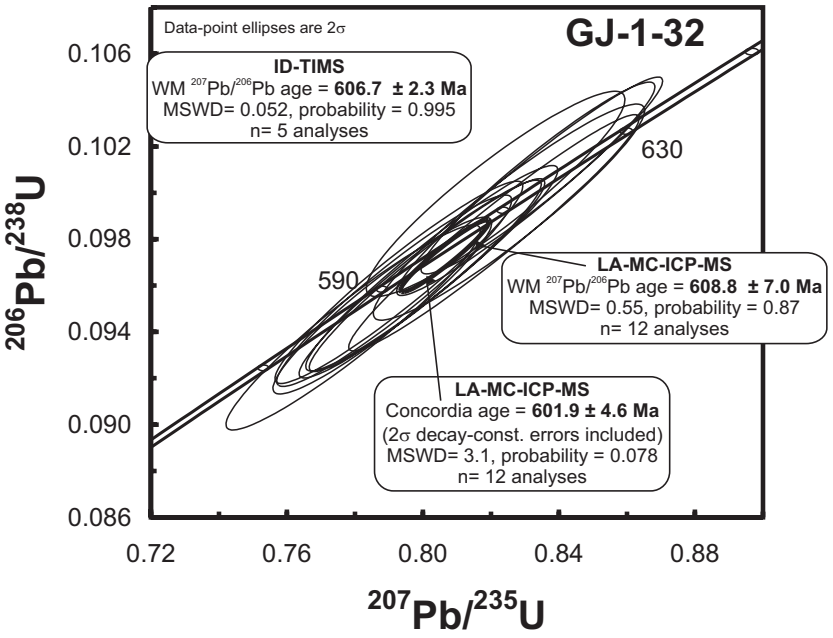

FIG. 15-13. Concordia plot containing the U–Pb dating results for zircon GJ1-32 obtained by LA–MC–ICP–MS using a 40 micrometre spot size. WM= weighted mean.

yielded a weighted mean $^{207}Pb/^{206}Pb$ age of 1305.3 ±2.2 Ma (2σ , Fig. 15-14a). LA–MC–ICP–MS analyses were conducted on one petrographic thin section of sample LH98-239 using the SuperCell™. The Pb–U LIEF was monitored by intermittent analysis of the in-house zircon standard LH94-15 located on a glass slide mount adjacent to the LH98-239 thin section. Figure 15-14a and Table 15-3 illustrate the U–Pb data obtained by LA–MC–ICP–MS analysis for a total of 18 analyses on 7 zircon samples. The 14 most concordant analyses yield a weighted mean $^{207}Pb/^{206}Pb$ age of 1304.1 ±5.7 Ma (2σ) or 'concordia age' of 1306.2 ± 6.2 Ma (2σ; Fig. 15-14a). The two LA–MC–ICP–MS and ID–TIMS ages are identical and once again corroborate the accuracy of the methodology employed in our lab. Of particular interest, the inset in Fig. 15-14a displays a high resolution back-scattered electron image of the petrological context in the immediate vicinity of euhedral zircon grain #6. The elongate, zircon crystal contains an appendage of pyrite; all are hosted by a larger ulvospinel grain that has exsolved to a trellis-textured intergrowth of magnetite and ilmenite. The fact that the U–Pb results from grain #6 are identical to those of the remaining zircon grains within the sample strongly suggests a genetic relationship between the sulfide mineralization and granite magmatism. This ability to document the textural context of the dated mineral highlights one of the principal advantages of the U–Pb protocol outlined here.

As with the previous sample, a glass slide mount containing zircon grains from sample GJ1-32

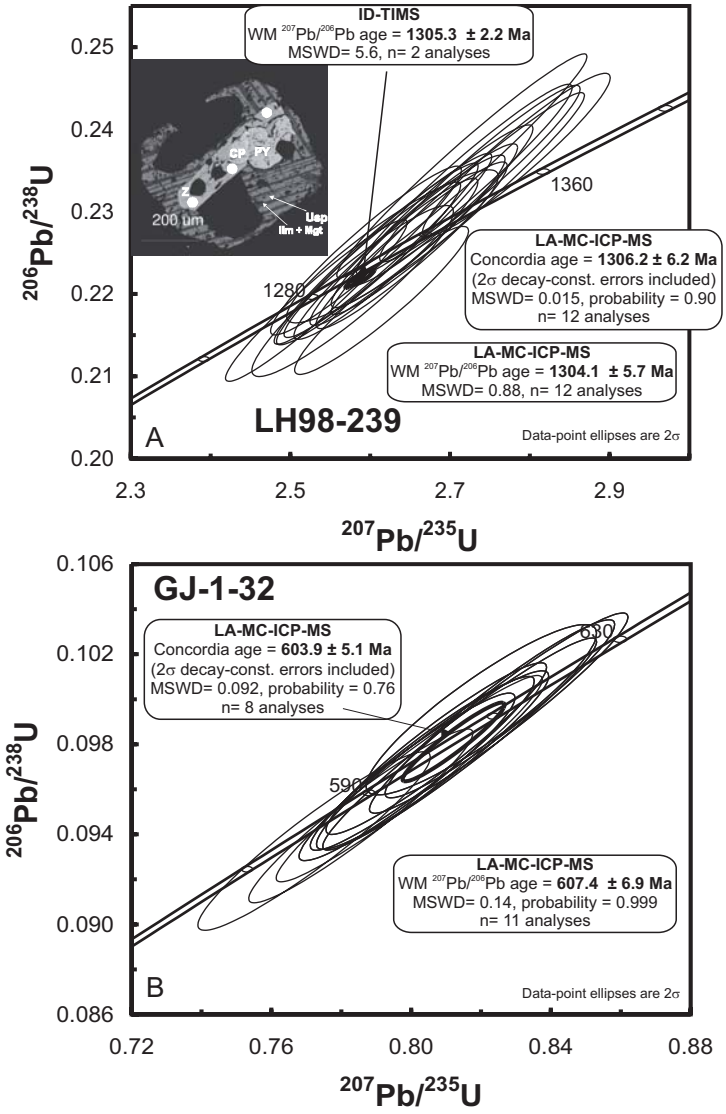

FIG. 15-14. Concordia plots illustrating the U–Pb age data for sample LH98-239, a clinopyroxene-fayalite granite from Voisey's Bay (**A**) obtained by ID–TIMS and LA–MC–ICP–MS, and (**B**) age results for GJ1-32 zircons using a spot size of 40 microns. Inset in (**A**) is a back-scattered electron image of the area within the petrographic thin section that surrounds zircon grain #6; z= zircon, CP= chalcopyrite, PY= pyrite, Usp= ulvospinel, Ilm= ilmenite, Mgt= magnetite. White circles represent locations of the laser ablation sites. WM= weighted mean. (**B**) Age results for GJ-1-32 zircons using a spot size of 40 microns.

was placed adjacent to the LH94-15 in-house zircon standard. Eleven laser ablation analyses using a 40 micron spot size yielded a weighted mean $^{207}Pb/^{206}Pb$ age of 607.4 ±6.9 Ma (2σ ; Fig. 15-14b). Once again, this result is indistinguishable from the LA–MC–ICP–MS data obtained during an earlier analytical session (Fig. 15-13) and ID–TIMS ages obtained at the University of Alberta and Macquarie University (Jackson *et al*. 2004).

Monazite: Queen Maud Block In a recent study, Schultz *et al*. (2007) report *in situ* U–Pb ages obtained on monazite and zircon in petrographic thin sections obtained by LA–MC–ICP–MS using the protocol described here. Granitoid and metasedimentary samples from the main lithologies of the Queen Maud block, located on the northwestern margin of the Rae province (Arctic Canada), were analyzed in order to understand better the tectonic history of northwestern Laurentia. In particular, monazite grains from three metasedimentary samples were investigated in order to delineate the timing of regional metamorphism.

U–Pb data for monazite from a sample of garnet-bearing migmatite leucosome (ST-3a) were obtained with the standard ablation cell, and are illustrated in Fig. 15-15 and listed in Table 15-3 (from Schultz *et al*. 2007). The Pb *versus* U LIEF was monitored using the Western Australia monazite standard (2842.9 ± 0.3 Ma; Heaman *et al*. unpublished ID–TIMS data). The data for sample ST-3a define a two-part history; cores from two monazite grains are characterized by patchy compositional zonation and mantled by compositionally homogeneous rims (Fig. 15-15). Laser ablation–MC–ICP–MS analyses of the cores conducted using a 12 μm spot size yielded a weighted mean $^{207}Pb/^{206}Pb$ age of 2481 ±7 Ma (2σ), which is coeval with the 2460 to 2500 Ma zircon ages obtained on granitoid rocks from the Queen Maud block. In contrast, LA–MC–ICP–MS analyses of rims (n=3) and homogeneous grains (n=10) yield a weighted mean $^{207}Pb/^{206}Pb$ age of 2385 ±5 Ma (Fig. 15-15). The *ca*. 2.5 Ga is

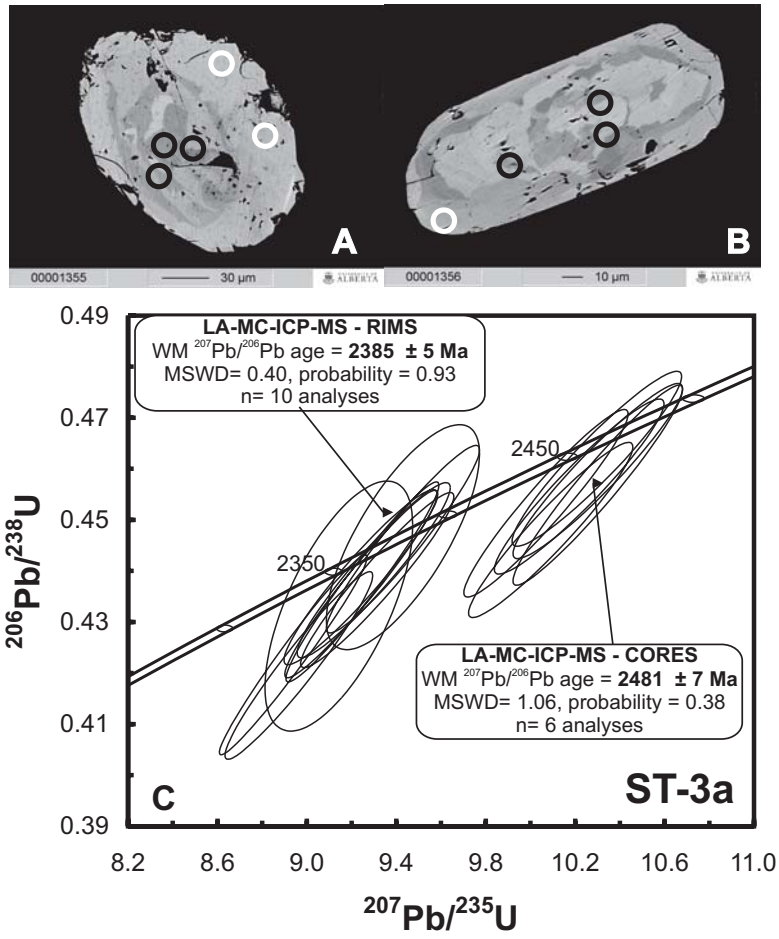

FIG. 15-15. (**A**) Back-scattered electron images of grain #3 and grain #4 (**B**) from sample ST-3a with locations of 12 μm ablation spots delineated; black open circles = core, white open circles = rim. (**C**) Concordia diagram that clearly illustrates the distinct age differences between cores and rims (diagram modified from Schultz *et al*., 2007).

interpreted as an igneous crystallization event, whereas the *ca*. 2.39 Ga most likely represents the timing of granulite-facies metamorphism since monazite with these ages occurs in melt leucosomes. Given the rather thin (~10 to 30 μm) nature of the metamorphic rims within the compositionally zoned monazite grains (Fig. 15-15), LA–MC–ICP–MS analysis of such grains in raster mode over a larger area would have resulted in geologically meaningless 'mixed' U–Pb ages (between ~2500 and ~2390 Ma). Hence, this study again demonstrates the importance of the 'reduced volume' approach.

Perovskite: Ice River Complex. Perovskite ($CaTiSiO_3$) is a useful mineral for dating mantle-derived melts of mafic or ultramafic (*e.g.*, kimberlite) and alkaline (*e.g.*, ijolite; Fig. 15-16) affinities since it occurs as a magmatic phase and is not known to record inheritance. Its occurrence in rocks of economic importance such as kimberlite has provided the impetus for geochronological investigations of perovskite using conventional isotope dilution methods (*e.g.*, Heaman & Kjarsgaard 2000) or SHRIMP analysis (*e.g.*, Kinney *et al*. 1997). However, successful dating of perovskite hinges upon the correction of the common Pb component. Recently, Cox & Wilton (2006) accurately dated perovskite from the Oka carbonatite by LA–ICP–MS using the 'Tera-Wasserburg' technique. This method involves calculating a regression line through uncorrected data on a measured $^{207}Pb/^{206}Pb$ *vs*. measured $^{238}U/^{206}Pb$ plot, *i.e.*, Tera-Wasserburg diagram (*e.g.*, Fig. 15-17a). The y-intercept value represents the $^{207}Pb/^{206}Pb$ ratio of the common Pb component; whereas the $^{207}Pb/^{206}Pb$ value of the radiogenic component is given by the age defined by the lower intersection of the regression line and the concordia curve. Both the radiogenic and common Pb $^{207}Pb/^{206}Pb$ values are used in the formula below to calculate the proportion of common Pb (f) for each analysis (after Compston *et al*. 1984):

$$f = \frac{\left(^{207}Pb/^{206}Pb_{measured} - {}^{207}Pb/^{206}Pb_{radiogenic}\right)}{\left(^{207}Pb/^{206}Pb_{common} - {}^{207}Pb/^{206}Pb_{radiogenic}\right)}$$

The latter approach was also adopted by Simonetti *et al*. (2006) to date titanite by LA–MC–ICP–MS successfully in petrographic thin section (*e.g.*, Banerjee *et al*. 2007), another accessory mineral that is characterized by a significant amount of common Pb. The reader is referred to the studies cited above for a detailed description of both the perovskite and titanite dating protocols using the 'Tera-Wasserburg' method.

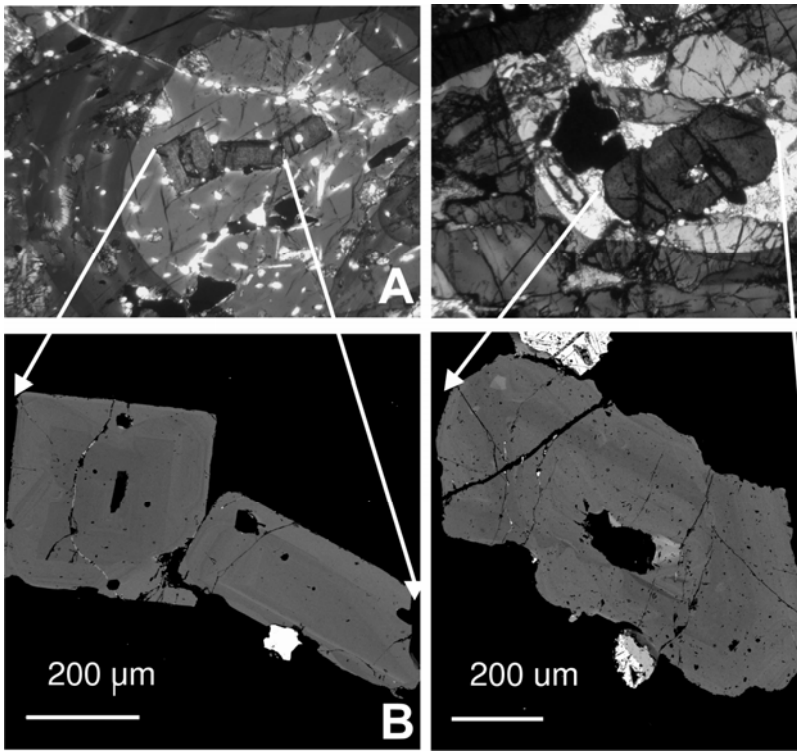

FIG. 15-16. Photomicrographs and back scattered electron images of perovskite grains taken from the petrographic thin section of sample I92-30 and subsequently analyzed by LA–MC–ICP–MS. **A**) and **B**) are pictures for grains labeled 2b and 2c in Table 15-4, whereas **C**) and **D**) represent images for grain 5 (Table 15-4).

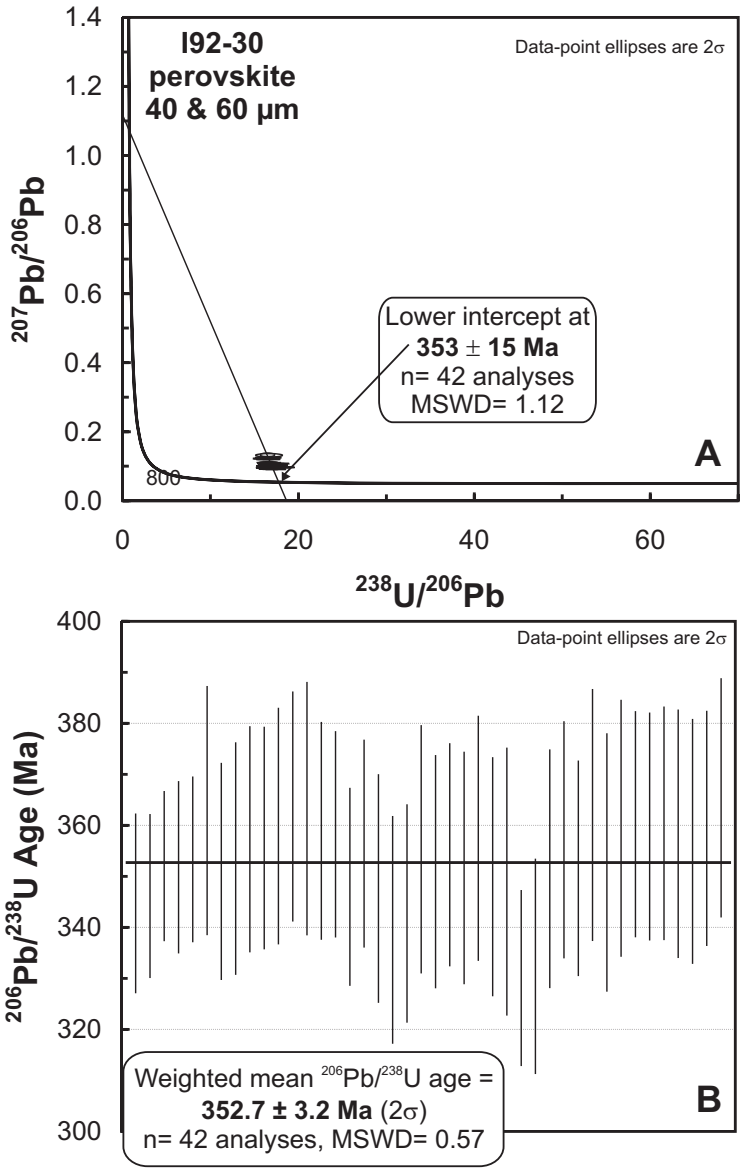

FIG. 15-17. **A**) Tera-Wassserburg plot illustrating the results obtained by LA–MC–ICP–MS for perovskite from the petrographic thin section of sample I92-30. **B**) Diagram depicting the individual, common Pb-corrected $^{206}Pb/^{238}U$ ages obtained for LA–MC–ICP–MS analyses of perovskite from sample I92-30 and corresponding calculated weighted mean age of 352.7 ± 3.2 Ma (2σ).

This analytical protocol was used to date perovskite within a sample of melteigite (Melanocratic end member of the ijolite series) from the Early Carboniferous Ice River ultramafic alkaline complex, British Columbia (Locock 1994, Pell & Höy 1989). The Ice River Complex is an arcuate shaped, zoned alkaline ultramafic intrusion covering an area ~30 km^2 and consists of two intrusive suites (from Pell & Höy 1989): an early, layered (feldspar-free) ijolite, jacupirangite, and urtite that is cored by a carbonatite plug and cut by carbonatite dykes; this was later intruded by a series of zoned syenite bodies associated with zeolitic and feldspathic carbonatite.

Six perovskite crystals from a petrographic thin section of sample I92-30, a perovskite-kaersutite-bearing melteigite (Fig. 15-16), were ablated predominantly at 40 µm for U–Pb age determination (Table 15-4; Fig. 15-17). The perovskite grains were ablated using the standard laser ablation cell and the Pb *vs*. U LIEF was monitored with repeated analysis of a perovskite external standard. The latter was also obtained from the Ice River Complex but from ijolite sample IR-6 (collected by T.D. Peterson, GSC Ottawa), which is characterized by abundant nepheline, clinopyroxene, perovskite with minor titanite, melanite garnet, apatite and ilmenite (pers. comm. from B. Kjarsgaard, GSC Ottawa). The external perovskite standard from sample IR-6 was dated by ID–TIMS

TABLE 15-4. U-PB LASER ABLATION DATA FOR ICE RIVER PEROVSKITE

Anal. #	Spot size (μm)	^{206}Pb cps	^{207}Pb/^{206}Pb	2σ uncert.	^{206}Pb/^{238}U meas.	2σ uncert.	% Rad. Pb	^{206}Pb/^{238}U corr.	2σ uncert.	^{206}Pb/^{238}U Age (Ma)	2σ uncert.
Gr 1 -1	60	282691	0.0574	0.0029	0.0995	0.0011	95.7	0.0549	0.0028	345	18
Gr 1 -2	60	318103	0.0575	0.0027	0.0972	0.0010	95.9	0.0552	0.0026	346	16
Gr 1 -3	60	338572	0.0607	0.0025	0.1331	0.0043	92.5	0.0561	0.0023	352	15
Gr 1b -4	60	311926	0.0586	0.0028	0.0987	0.0010	95.8	0.0561	0.0027	352	17
Gr 1b -5	60	296524	0.0587	0.0027	0.0968	0.0010	95.9	0.0563	0.0026	353	16
Gr 2a -6	40	156959	0.0603	0.0041	0.0960	0.0010	96.0	0.0579	0.0039	363	24
Gr 2a -7	40	156225	0.0584	0.0035	0.0982	0.0011	95.8	0.0560	0.0034	351	21
Gr 2a -8	40	170053	0.0590	0.0038	0.1017	0.0012	95.5	0.0564	0.0036	353	23
Gr 2b -9	40	156842	0.0595	0.0037	0.0982	0.0011	95.8	0.0570	0.0035	357	22
Gr 2b -10	40	160258	0.0596	0.0036	0.0989	0.0010	95.7	0.0570	0.0035	358	22
Gr 2b -11	40	164301	0.0600	0.0039	0.0999	0.0011	95.7	0.0574	0.0037	360	23
Gr 2c -12	40	171447	0.0607	0.0038	0.1001	0.0011	95.6	0.0580	0.0036	364	23
Gr 2c-13	40	147706	0.0603	0.0041	0.0951	0.0010	96.1	0.0580	0.0040	363	25
Gr 3a-14	40	158686	0.0596	0.0035	0.0960	0.0010	96.0	0.0573	0.0034	359	21
Gr 3a-15	40	153350	0.0603	0.0034	0.1094	0.0032	94.8	0.0571	0.0032	358	20
Gr 3a-16	40	214423	0.0575	0.0032	0.0910	0.0010	96.5	0.0555	0.0031	348	19
Gr 3a-17	40	217238	0.0599	0.0034	0.1075	0.0011	94.9	0.0568	0.0033	356	20
Gr 3b-18	40	246560	0.0583	0.0038	0.1059	0.0012	95.1	0.0554	0.0036	348	22
Gr 3b-19	40	186671	0.0570	0.0037	0.1075	0.0012	94.9	0.0541	0.0036	340	22
Gr 3b-20	40	173684	0.0573	0.0036	0.1041	0.0017	95.3	0.0546	0.0034	343	21
Gr 4a-21	40	159137	0.0604	0.0041	0.1201	0.0013	93.8	0.0567	0.0039	355	24
Gr 4a-22	40	167574	0.0584	0.0038	0.0978	0.0011	95.8	0.0559	0.0036	351	23
Gr 4a-23	40	161580	0.0590	0.0036	0.0993	0.0011	95.7	0.0565	0.0035	354	22
Gr 4a-24	40	189951	0.0584	0.0038	0.0956	0.0010	96.1	0.0561	0.0036	352	23
Gr 4a-25	40	157063	0.0597	0.0040	0.1008	0.0014	95.6	0.0570	0.0038	357	24
Gr 4b-26	40	150064	0.0582	0.0039	0.0985	0.0010	95.8	0.0558	0.0037	350	23
Gr 4b-27	40	166885	0.0600	0.0045	0.1316	0.0041	92.7	0.0556	0.0042	349	26
Gr 4c-28	40	151734	0.0548	0.0029	0.0970	0.0012	95.9	0.0525	0.0027	330	17
Gr 4c-29	40	164872	0.0551	0.0035	0.0965	0.0011	96.0	0.0529	0.0034	332	21
Gr 5-30	40	160266	0.0586	0.0039	0.1002	0.0011	95.6	0.0560	0.0037	351	23
Gr 5-31	40	160920	0.0600	0.0039	0.1071	0.0014	95.0	0.0570	0.0037	357	23
Gr 5-32	40	177411	0.0588	0.0035	0.1037	0.0011	95.3	0.0561	0.0034	352	21
Gr 5-33	40	157318	0.0617	0.0042	0.1220	0.0021	93.6	0.0578	0.0039	362	25
Gr 5-34	40	173758	0.0603	0.0043	0.1247	0.0014	93.3	0.0562	0.0040	353	25
Gr 5-35	40	152028	0.0597	0.0042	0.0960	0.0011	96.0	0.0573	0.0040	359	25
Gr 6a-36	40	158165	0.0599	0.0037	0.0971	0.0010	95.9	0.0575	0.0035	360	22
Gr 6a-37	40	171996	0.0595	0.0037	0.0917	0.0010	96.4	0.0574	0.0036	360	22
Gr 6a-38	40	163006	0.0602	0.0038	0.1011	0.0011	95.5	0.0575	0.0037	360	23
Gr 6a -39	40	166792	0.0597	0.0041	0.0993	0.0017	95.7	0.0572	0.0039	358	24
Gr 6a -40	40	179446	0.0601	0.0040	0.1099	0.0014	94.7	0.0569	0.0038	357	24
Gr 6b -41	40	166895	0.0597	0.0038	0.0965	0.0010	96.0	0.0573	0.0037	359	23
Gr 6b -42	40	162029	0.0608	0.0039	0.0962	0.0010	96.0	0.0583	0.0037	365	23

and has yielded an age of 356.4 ± 1.1 Ma (2σ; n= 8 analyses; Heaman *et al*., in prep.). A total of 42 laser ablation analyses of perovskite from sample I92-30 define a lower intercept of 353 ± 15 Ma (2σ; Fig. 15-17a) and a weighted mean $^{206}Pb/^{238}U$ age of 352.7 ± 3.2 Ma (2σ; Fig. 15-17b). This date corroborates the ID–TIMS age results obtained on the IR-6 external perovskite standard (356.4 ± 1.1 Ma) and that of 356.2 ± 5.9 Ma (2σ) based on analyses of mineral separates of pyrochlore, perovskite, and schorlomite from various intrusive phases of the Ice River Complex (Locock 1994).

SUMMARY

The U–Pb protocol described here involving the use of a unique collector array consisting of a combination of three discrete-dynode electron multipliers and twelve Faraday collectors provides distinct advantages for U–Pb dating of accessory mineral phases by LA–MC–ICP–MS. These are:

1. Measurement of the ^{207}Pb, ^{206}Pb, and ^{204}Pb ion signals using the three electron multipliers allows for the laser ablation of a number of accessory phases to be conducted at low fluence and hence consumes much less sample volume without lowering the precision of the $^{207}Pb/^{206}Pb$ analyses. This '*reduced volume*' approach readily allows for the U–Pb dating of accessory phases including zircon, monazite, titanite and perovskite within standard petrographic thin sections. The capacity to date accessory minerals precisely and accurately in their petrological context is invaluable for resolving a wide range of geological questions.
2. The typical 2σ uncertainty associated with measurement of the $^{207}Pb/^{206}Pb$ value with our LA–MC–ICP–MS protocol is lower than that typically obtained by SHRIMP. The 2σ uncertainty associated with the calculated weighted mean $^{207}Pb/^{206}Pb$ age approaches that obtained by ID–TIMS. Thus, the analytical protocol described here is certainly more cost-effective than either of these two methods.
3. The comparative laser ablation tests conducted using either the standard or SuperCell™ ablation cells seem to yield similar performances relative to sensitivity, signal 'washout', and overall quality of the U–Pb data. The important advantage of the SuperCell™ relative to the standard laser ablation cell is its capacity to incorporate glass mounts containing matrix-matched standards simultaneously. This enables more frequent monitoring of the Pb *versus* U laser induced element fractionation during a single analytical session and also increases sample through-put.
4. When using a combination of discrete-dynode electron multipliers and Faraday collectors for U–Pb age dating by LA–MC–ICP–MS, high quality data is achievable when the ion-counting devices are properly calibrated relative to one another, and against the Faraday bucket recording the ^{238}U ion signal.

ACKNOWLEDGEMENTS

The radiogenic isotope facility at the University of Alberta is partly supported by a NSERC MRS grant. We thank Jason Cameron, GuangCheng Chen, Gayle Hatchard, Mark Labbe, Don Resultay, and Judy Schultz for technical assistance. We are extremely grateful to Andrew Locock for providing sample I92-30 from his MSc thesis collection and discussions relating to the dating of common Pb–bearing accessory minerals. We thank Adam Kent and an anonymous reviewer for providing constructive comments.

REFERENCES

ASHTON, K.E., HEAMAN, L.M., LEWRY, J.F., HARTLAUB, R.P. & SHI, R. (1999): Age and origin of the Jan Lake Complex ; a glimpse at the buried Archean craton of the Trans-Hudson orogen. *Can. J. Earth Sci.* **36**, 105-208.

BANERJEE, N.R., SIMONETTI, A., FURNES, H., MUELENBACHS, K., STAUDIGEL, H., HEAMAN, L. & VAN KRANENDONK, M.J. (2007): Direct dating of Archean microbial ichnofossils. *Geology* **35**, 487-490.

CHENERY, S. & COOK, J.M. (1993): Determination of rare earth elements in single mineral grains by laser ablation microprobe-inductively coupled plasma mass spectrometry-preliminary study. *J. Anal. At. Spectrom.* **8**, 299-303.

COMPSTON, W., WILLIAMS, I.S. & MEYER, C.E. (1984): U–Pb geochronology of zircons from lunar breccia 73217 using a sensitive high mass-resolution ion microprobe. *J. Geophys. Res*. **B89**, 525-534.

COX, R.A. & WILTON, D.H.C. (2006): U–Pb dating of perovskite by LA–ICP–MS: An example from the Oka carbonatite, Quebec, Canada. *Chem. Geol*. **235**, 21-32.

COX, R.A., WILTON, D.H.C. & KOŠLER, J. (2003): Laser-ablation U–Th–Pb *in situ* dating of zircon

and allanite: An example from the October Harbour granite, central coastal Labrador, Canada. *Can. Mineral.* **41**, 273-291.

DUNSTAN, L.P., GRAMCH, J.W., BARNES, I.L. & PURDY, W.C. (1980): Absolute isotopic abundance and the atomic weight of a reference sample of thallium. *J. Res. National Bureau of Standards* **85**, 1-10.

EGGINS, S.M., KINSLEY, L.P.J. & SHELLEY, J.M.G. (1998): Deposition and element fractionation processes during atmospheric pressure laser sampling for analysis by ICP–MS. *Appl. Surf. Sci.* **127-129**, 278-286.

GÜNTHER, D., COUSIN, H., MAGYAR, B. & LEOPOLD, I. (1997): Calibration studies on dried aerosols for laser ablation-inductively coupled plasma mass spectrometry. *J. Anal. At. Spectrom.* **12**, 165-170.

HEAMAN, L.M. & KJARSGAARD, B.A. (2000): Timing of eastern North American kimberlite magmatism; continental extension of the Great Meteor Hotspot track? *Earth Planet. Sci. Lett.* **178**, 253-268.

HOFFMANN, D.L., RICHARDS, D.A., ELLIOT, T.R., SMART, P.L., COATH, C.D. & HAWKESWORTH, C.J. (2005): Characterization of secondary electron multiplier nonlinearity using MC–ICPMS. *Int. J. Mass Spectrom.* **244**, 97-108.

HORN, I., RUDNICK, R.L. & MCDONOUGH, W.F. (2000): Precise elemental and isotope ratio determination by simultaneous solution nebulization and laser ablation–ICP–MS: application to U–Pb geochronology. *Chem. Geol.* **164**, 281-301.

HORSTWOOD, M.S.A. (2008): Data reduction strategies, uncertainty assessment and resolution of LA–MC–ICP–MS isotope data. *Mineralogical Association of Canada Short Course Series Volume* **40**, xx-xx (this volume).

HORSTWOOD, M.S.A., FOSTER, G.L., PARRISH, R.R., NOBLE, S.R. & NOWELL, G.M. (2003): Common-Pb corrected *in situ* U–Pb accessory mineral geochronology by LA–MC–ICP–MS. *J. Anal. At. Spectrom.* **18**, 837-846.

JACKSON, S.E., PEARSON, N.J., GRIFFIN, W.L. & BELOUSOVA, E.A. (2004): The application of laser ablation-inductively coupled plasma–mass spectrometry to *in situ* U–Pb geochronology. *Chem. Geol.* **211**, 47-69.

JAFFEY, A.H., FLYNN, K.F., GLENDENIN, L.E., BENTLEY, W.C. & ESSLING, A.M. (1971): Precision measurement of half-lives and specific activities of 235U and 238U. *Physical Rev.* **4**, 1889-1906.

JEFFRIES, T.E., FERNANDEZ-SUAREZ, J., CORFU, F. & Gabriel Gutierrez, A. (2003): Advances in U–Pb geochronology using a frequency quintupled Nd:YAG based laser ablation system (λ = 213) and quadrupole based ICP–MS. *J. Anal. At. Spectrom.* **18**, 847-855.

KINNEY, P.D., GRIFFIN, B.J., HEAMAN, L.M., BRAKHFOGEL, F.F. & SPETSIUS, Z.V. (1997): SHRIMP U–Pb ages of perovskite from Yakutian kimberlites. *Russ. Geol. Geophys.* **38**, 97-105.

LABERGE, J.D. & PATTISON, D.R.M. (2007): Geology of the western margin of the Grand Forks complex, southern British Columbia: high-grade Cretaceous metamorphism followed by early Tertiary extension of the Granby fault. *Can. J. Earth Sci.* **44**, 199-228.

LEMIEUX, Y., THOMPSON, R.J., ERDMER, P., SIMONETTI, A. & CREASER, R.A. (2007): Detrital zircon geochronology and provenance of Late Proterozoic and mid-Paleozoic successions outboard of the miogeocline, southeastern Canadian Cordillera. *Can. J. Earth Sci.* **44**, 1675-1693.

LOCOCK, A.J. (1994): Aspects of the geochemistry and mineralogy of the Ice River Alkaline Intrusive Complex, Yoho National Park, British Columbia. University of Alberta, MSc thesis, 163 pages.

LUDWIG, K.R. (2003): User's manual for Isoplot 3.00: A geochronological toolkit for Microsoft Excel. *Berkeley Geochronology Center Special Publication* No. **4**, 70 pages.

MILLER, J.S., SANTOSH, M., PRESSLEY, R.A., CLEMENTS, A.S. & ROGERS, J.J.W. (1996): A Pan-African thermal event in southern India. *J. Southeast Asian Earth Sci.* **14**, 127-136.

PAUL, B., WOODHEAD, J.D. & HERGT, J. (2005): Improved *in situ* isotope analysis of low-Pb materials using LA–MC–ICP–MS with parallel ion counter and Faraday detection. *J. Anal. At. Spectrom.* **20**, 1350-1357.

PELL, J. & HÖY, T. (1989): Carbonatites in a continental margin environment – the Canadian Cordillera. *In* Carbonatites: Genesis and Evolution (K. Bell, *ed.*). Unwin Hyman, London, 200-220.

RICHTER, S., GOLDBERG, S.A., MASON, P.B., TRAINA, A.J. & SCHWIETERS, J.B. (2001): Linearity tests for secondary electron multipliers used in isotope ratio mass spectrometry. *Int. J. Mass Spectrom.* **206**, 105-127.

SCHULTZ, M.E.J., CHACKO, T., HEAMAN, L.M., SANDEMAN, H.A., SIMONETTI, A. & CREASER, R.A. (2007): Queen Maud Block: A newly recognized Paleoproterozoic (2.4–2.5 Ga) terrane in northwest Laurentia. *Geology* **35**, 707-710.

SIMONETTI, A., HEAMAN, L.M., HARTLAUB, R.P., CREASER, R.A., MACHATTIE, T.G. & BÖHM, C. (2005): U–Pb zircon dating by laser ablation–MC–ICP–MS using a new multiple ion counting Faraday collector array. *J. Anal. At. Spectrom.* **20**, 677-686.

SIMONETTI, A., HEAMAN, L.M., CHACKO, T. & BANERJEE, N.R. (2006): *In situ* petrographic thin section U–Pb dating of zircon, monazite, and titanite using laser ablation–MC–ICP–MS. *Int. J. Mass Spectrom.* **253**, 87-97.

SOUDERS, A.K. & SYLVESTER, P.J. (2008a): *Mineralogical Association of Canada Short Course Series Volume* **40**, xx-xx (this volume).

SOUDERS, A.K. & SYLVESTER, P.J. (2008b): Improved *in situ* measurements of lead isotopes in silicate glasses by LA–MC–ICPMS using multiple ion counters. *J. Anal. At. Spectrom.* **23**, 535-543.

STEIGER, R.H. & JÄGER, E. (1975): Subcommission on geochronology: convention on the use of decay constants in geo- and cosmochronology. *Earth Planet. Sci. Lett.* **36**, 359-362.

STERN, R.A. (2001): A new isotopic and trace element standard for the ion microprobe: preliminary thermal ionization mass spectrometry (TIMS) U–Pb and electron microprobe data. *Geol. Surv. Canada, Current Research* 2001-F1.

STERN, R.A. & AMELIN, Y. (2003): Assessment of errors in SIMS zircon U–Pb geochronology using a natural zircon standard and NIST SRM 610 glass. *Chem. Geol.* **197**, 111-142.

TAYLOR, R.N., WARNEKE, T., MILTON, J.A., CROUDACE, I.W., WARWICK, P.E. & NESBITT, R.W. (2003): Multiple ion counting determination of plutonium isotope ratios using multi-collector ICP–MS. *J. Ana. At. Spectrom.* **18**, 480-484.

TODT, W., CLIFF, R.A., HANSER, A. & HOFMANN, A.W. (1996): Evaluation of a ^{202}Pb–^{205}Pb double spike for high-precision lead isotope analysis. In : Earth Processes. Reading the Isotope Code. Geophysical Monograph **95**. Ed. A. Basu, American Geophysical Union, Washington, 429-437.

WIEDENBECK, M., ALLÉ, P., CORFU, F., GRIFFIN, W.L., MEIER, M., OBERLI, F., VON QUADT, A., RODDICK, J.C. & SPIEGEL, W. (1995): Three natural zircon standards for U–Th–Pb, Lu–Hf, trace element and REE analyses. *Geostand. Newsl.* **19**, 1-23.

WILLIGERS, B.J.A., BAKER, J.A., KROGSTAD, E.J. & PEATE, D.W. (2002): Precise and accurate *in situ* Pb–Pb dating of apatite, monazite, and sphene by laser ablation multiple-collector ICP–MS. *Geochim. Cosmochim. Acta* **66**, 1051-1066.